Light-Interacting iron-based nanomaterials for localized cancer detection and treatment

Edouard Alphandéry

Light-Interacting Iron-Based Nanomaterial For Localized Cancer Detection and Treatment

Edouard Alphandéry[+,++,+++]

[+]Sorbonne Université, Muséum National d'Histoire Naturelle, UMR CNRS 7590, IRD, Institut de Minéralogie, de Physique des Matériaux et de Cosmochimie, IMPMC, 75005 Paris, France

[++]Nanobacterie SARL, 36 boulevard Flandrin, 75116, Paris, France.

[+++]Institute of Anatomy, UZH University of Zurich, Instiute of Anatomy, Winterthurerstrasse 190, CH-8057, Zurich, Switzerland.

Email address: edouardalphandery@hotmail.com, phone: 0033632697020

ABSTRACT: To improve the prognosis of cancer patients, methods of local cancer detection and treatment could be implemented. For that, iron-based nanomaterials (IBN) are particularly well-suited due to their biocompatibility and the various ways in which they can specifically target a tumor, *i.e.* through passive, active or magnetic targeting. Furthermore, when it is needed, IBN can be associated with well-known fluorescent compounds, such as dyes, clinically approved ICG, fluorescent proteins, or quantum dots. They may also be excited and detected using well-established optical methods, relying on scattering or fluorescent mechanisms, depending on whether IBN are associated with a fluorescent compound or not. Systems combining IBN with optical methods are diverse, thus enabling tumor detection in various ways.. In addition, these systems provide a wealth of information, which is inaccessible with more standard diagnostic tools, such as single tumor cell detection, in particular by combining IBN with near-field scanning optical microscopy, dark-field microscopy, confocal microscopy or super-resolution microscopy, or the highlighting of certain dynamic phenomena such as the diffusion of a fluorescent compound in an organism, *e.g.* using fluorescence lifetime imaging, fluorescence resonance energy transfer, fluorescence anisotropy, or fluorescence tomography. Furthermore, they can in some cases be complemented by a therapeutic approach to destroy tumors, *e.g.* when the fluorescent compound is a drug, or when a technique such as photo-thermal or photodynamic therapy is employed. This review brings forward the idea that iron-based nanomaterials may be associated with various optical techniques to form a commercially available toolbox, which can serve to locally detect or treat cancer with a better efficacy than more standard medical approaches.

KEYWORDS:

Iron-based nanomaterials, oncology, cancer, optical methods, fluorescence, nano, fluorescent nanoparticles, nanomedicine.

ABREVIATIONS:

λ: wavelength used to excite the fluorescent compound associated to the iron-based nanomaterial;

AF: Alexa fluor;

AFM: Atomic force microscopy;

BBB: Blood brain barrier;

BP: Body part;

CAs: Cerebral aneurysms;

CCD: Charge-coupled device;

CD: carbon dot;

Cy: Cyanine;

ctDNA: cicrculating tumor DNA ;

CT: computed tomography;

CTDR: Cell Tracker Deep Red;

CM: confocal microscopy;

CTC: Circulating tumor cells;

DAPI: 4',6-diamdino-2phenylindeo;

DFM: Dark field microscopy;

DiI: 1,1′-dioctadecyl-3,3,3′,3′-tetramethylindocarbocyanine;

DMSA: Dimercaptosuccinic acid

DOX: Doxorubicin;

EpCAM: epithelial cell adhesion molecule;

EPI: Epirubicin;

EPR effect: Enhanced permeability and retention effect;

FA: Fluorescence anisotropy;

FC: Fluorescent compound;

FDR: fluorescent decay rate;

FGS: Fluorescence guided surgery;

FI: Fluorescence imaging;

FLIM: Fluorescence lifetime imaging;

FIBN: Fluorescent iron-based nanomaterials;

FITC: Fluorescein isothiocyanate;

FLIM: Fluorescence lifetime imaging;

FRET: Fluorescence resonance energy transfer;

GBM: Glioblastoma multiform;

GFP: Green fluorescent protein;

HD: Hydrodynamic diameter;

HS: Hydrodynamic size;

IBN: Iron based nanomaterials;

IONP: Iron oxide nanoparticles;

IR: Infra-red

ICG: Indocyanine green;

LB: Liquid biopsy;

LSPR: Localized surface plasmon resonance;

MHT: Magnetic hyperthermia;

MRI: Magnetic resonance imaging;

NFIBN: Non-fluorescent iron-based nanomaterials;

NP: Nanoparticles;

NSOM: Near-field optical microscopy;

PDT: Photodynamic therapy;

PEI: Polyethylenimine;

PEG: Polyethylene glycol;

PFR: Phenol Formaldehyde Resin;

PL: Photoluminescence;

PMA: Poly(methyl acrylate);

PMT: Photo multiplier;

PS: Photosensitizer;

PTT: Photo-thermal therapy;

PVLA: Polyvinylbenzyl-O-beta-D-galactopyranosyl-D-gluconamide;

QD: Quantum dot;

RhB: Rhodamine B;

RITC: Rhodamine B isothiocyanate;

SAXS: Small angle X-ray diffraction;

SERS: Surface enhanced Raman spectroscopy;

SIM: Structured illumination microscopy;

SPECT: Single photon emission computed tomography;

SPM: Single photon microscopy;

SPION: Superparamagnetic iron oxide nanoparticle;

TPM: Two photon microscopy;

US: Ultrasound;

WFEM: Wide field epifluorescence microscopy;

XRD: X-ray diffraction;

INTRODUCTION

To improve the prognostic of cancer patients, two inter-connected aspects deserve to be considered, *i.e.* first, cancer should be detected at the earliest possible stage, and second, tumors should be treated locally when they are sufficiently small, non-invasive, and non-metastatic. This double aim can be achieved by using nanomaterials that specifically target tumor cells and are detected or excited locally by various optical methods, [1]. Among the different types of markers, iron based nanomaterials (IBN) present a large number of advantages characterized by: i) their ability to detect a wide range of different cancer biomarkers, *e.g.* tumor cells, Protein, ctDNA, microRNA, DNA methylation, circulating tumor cells, [2], ii) their contrasting properties in various traditional cancer detection techniques, such as computed tomography (CT), Magnetic Resonance Imaging (MRI), Ultrasound (US), where they yield improved sensitivity, [3], iii) their faculty to act as multimodal imaging tools, [4], notably in magnetic resonance imaging (MRI), (5), single-photon emission computed tomography (SPECT), [6], X-Ray diffraction (XRD), [7, 8], or Small-Angle X-Ray Scattering (SAXS), [9], iv) their biocompatibility, *i.e.* they were safely administered to humans and used in the clinic either as contrast agents, or for the treatment of iron anemia diseases, [10], v) their capability to locally heat tumors, *e.g.* through magnetic hyperthermia (MHT), [11, 12], or photo-thermal therapy (PTT), [13], vi) their movement in the organism that can be adjusted via the application of an external magnetic field, [14], vii) their potential to target tumor, *e.g.* through passive targeting via enhanced permeability and retention (EPR) effect or active targeting by attaching to IBN a molecule that specifically recognizes a tumor cell receptor, [15], and viii) their capacity to carry a chemotherapeutic drug or photosensitizer (PS) to tumor site, [16]. Two types of IBN can be distinguished. The first one consists of non-fluorescent IBN, whose properties are reviewed elsewhere both for naturally and chemically synthesized IBN, [17, 18]. They can be used as nanoscale local detector tools operating through a light scattering mechanism. The second one, designated as FIBN, comprises iron-based nanomaterials associated with a fluorescent compound. FIBN can be used in various fluorescence imaging techniques and are most often conceived to avoid fluorescence quenching by iron

oxide, *e.g.* by introducing an intercalating material between the fluorescent compound and the iron complex, which is characterized by a wide band gap or a thickness that is sufficiently thick to avoid electron transfer between the fluorescent compound and the iron-based nanomaterial, [19, 20, 21]. Recent studies have also introduced FIBN working through another mechanism of fluorescence de-quenching upon release of the fluorescence substance from FIBN magnetic core, [22, 23]. It enables visualizing the release of the fluorescence substance from the nanoparticle, a mechanism that is especially interesting when the fluorescence substance is a drug whose activity is triggered upon release. Here, the various types of light detection methods operating in combination with IBN/FIBN are described as well as their applications in the oncology field. Most of them operate in the infrared (IR), since fluorescent compounds often absorb/emit light within this range of wavelengths, light tissue penetration is enhanced at IR long wavelengths, and tissue absorption can be partly avoided in the IR, specifically between 650 and 900 nm, where tissue autofluorescence and water/hemoglobin absorptions are minimized, [24]. In addition to being able to optically detect tumors, FIBN can be used in light-induced cancer treatment, essentially through PDT or PTT. This review covers the description of optical methods operating within the tissular/cellular environment in the visible/infrared region for which most scattering/fluorescent mechanisms are reported to occur. Characterizations methods used to estimate IBN sizes, shapes, compositions outside of their biological environment, such as X-RD, [25, 8, 26, 9, 7, 27], SAXS, [28], dynamic light scattering (DLS), [29-31], FT-IR, [32-34], or optical-based techniques operating in the UV or radio-frequency wavelength range, such as SPECT, CT, or MRI, are described in other detailed reviews, [4].

I. OPTICAL PROPERTIES OF IRON OXIDE NANOPARTICLES

Iron oxide nanoparticles (IONP), composed of maghemite (γFe_2O_3) or magnetite (Fe_3O_4), are the most commonly studied IBN. Generally, they significantly absorb light between 200 and 600-800 nm, and display an absorption strength that strongly increases with decreasing wavelength, displaying specific absorption bands at 400 and 420 nm for Fe_3O_4 and 300 nm for γFe_2O_3, [35]. In addition, IONP can yield

photoluminescence (PL), although such effect was rarely reported, most probably due to a weak PL signal. In one study, IONP with sizes lying between 10 nm and 5 μm were observed to display PL peaks at 560 nm, 695 nm, and 840 nm, under excitation at 350 and 407 nm. These peaks were attributed to various recombination of electrons at IONP tetrahedral and octahedral sites, [36]. Furthermore, IONP has a band structure that directly impacts its fluorescence properties. Indeed, the presence of an unfilled shell of Fe^{3+} and Fe^{2+} at IONP surface, [37], where electrons can transfer from the fluorescent compound (FC) attached to them, leads to a mechanism of fluorescence quenching under laser excitation, [38]. As described in the next section, strategies have been employed to develop various FIBN, in which this quenching mechanism is suppressed. Light interaction with IBN can also lead to a scattering phenomenon, which is enhanced when the incident light couples with so-called surface plasmon waves. This is the reason why, when the detection of a scattering signal is sought for, the surface of IBN is often adjusted to result in an efficient surface plasmon wave effect. To this end, it was suggested to design mixed structures containing iron with a plasmonic material (gold or silver), *i.e.* by incorporating iron in Au NP (nanoparticle), [39], by designing gold–iron oxide Janus magnetic–plasmonic nanoparticles, [40], by coating IBN with gold, [41], or silver, [42]. Although the nature of the material located at IBN surface appears crucial to optimize the plasmonic effect, other parameters should also be taken into consideration for such endeavor, such as the shape, size, and type of assembly/interactions of IBN, [43].

II. DIFFERENT TYPES OF FLUORESCENT IRON-BASED NANOMATERIALS

Fluorescent iron-based nanomaterials (FIBN), whose composition, type of assembly, fluorescent properties, and various operating mechanisms are summarized in table 1 and Figure 1, consist of a first metallic part, which is composed of γFe_2O_3 (maghemite) or Fe_3O_4 (magnetite), or of an alloy made of iron mixed with different metals, such as cobalt ferrite, FePt, or Zinc ferrite. Concerning pure iron oxides, although most studies report that they are composed of magnetite, it is possible that they in fact consist of maghemite, since on the one hand magnetite should oxidize into maghemite in the absence of a specific treatment/layer protecting magnetite against oxidation, and on the other hand magnetite and maghemite

structures are very close to each other, *i.e.* their electron diffraction patterns are very similar, [44], making these two structures difficult to distinguish one from the other in the absence of a specific characterization method such as Raman scattering, [45]. Maghemite is very stable and should not be prone to a phase transition in the absence of a specific harsh treatment such as heating at 900 °C, which can oxidize maghemite into hematite, [34]. Cobalt ferrite composition presents the advantage of yielding improved magnetic properties, [46]. Although preliminary assessment of the toxicity of cobalt doped IBN led to a reassuring safety profile, [46], it is not certain that regulatory agencies will allow their administration to humans due to the well-known toxicity of cobalt, [47]. FePt has shown good biocompatibility, resistance to oxidation, and high chemical stability [368], while the doping of ferrite with zinc increases IBN magnetization values, [48].

Besides their metallic portion, FIBN comprise a fluorescent part that can be classified in four different categories. The first one consists of classic fluorescent compounds, mainly dyes or fluorescent proteins, *e.g.* ICG, [16], RhB, [49-,51], RITC, [52-55], Cy, [56-58], ATTO, [59, 60], fluorescein/FITC, [61-68], which usually emit/absorb in the visible, near infrared or far infrared, *i.e.* mainly between 380 and 1000 nm. Among all these compounds, ICG presents the advantage of being authorized for human injection for a number of imaging applications, [69], hence suggesting that FIBN comprising ICG may be authorized for clinical application provided their safety is established. The second one is made of quantum/carbon dots, [70-87], whose absorption/emission wavelengths vary between 200 and 800 nm depending on their composition and size. These materials present the advantages of displaying absorption/emission peaks with wavelengths that can be tuned through size adjustment and stock shifts that are often larger than for dyes due to light quantum confinement. These properties yield efficient imaging. However, some of these materials also suffer from the presence of toxic elements in their composition, *e.g.* CdSe, [72, 88, 77, 89], CdTe, [90, 91, 77, 75], CdSe/CdS, [70], CdSe/ZnS, [72, 83], CdTe/ZnS, [73], CdTe/CdSe, [76], CdTe/CdS, [79], ZnS, [81], and from a blinking effect, *i.e.* intermittent light emission, [92]. The third type of fluorescent materials consists of luminescence up-conversion compounds such as Yb^{3+}/Er^{3+}, [93], Yb^{3}

$^{+}$/Tm^{3+} co-doped $NaYF_4$, [93], $NaYF_4$:Yb, Er, [94], which emit light at shorter wavelength than their excitation wavelength. The use of long excitation wavelengths with large tissue penetration paves the way towards deep *in vivo* fluorescence. Fourth, metallic compounds different from iron such as chromium can be incorporated in FIBN, *e.g.* in Cr_2O_3 FIBN, and yield fluorescent properties with emission/absorption at 460 nm/360 nm, [95].

Metallic and fluorescent compounds are assembled together to form a complex in the following different manners. In most cases, a fluorescent compound is attached to the metallic part of the complex, either directly, *i.e.* without an intermediate layer [72, 88, 54], or via a coating made of various organic layers such as chitosan, [63], carboxy-methyl-chitosan, [63, 73], dextran, [79], DMSA, [49], PEI, [96], polyelectrolytes, [75], PLMA, [32], PEG, [16, 55], or inorganic compounds such as SiO_2, [95, 97, 70, 52, 93, 98, 99]. The coating can be made of a single layer/matrix, *e.g.* of silica, [100], or of several layers, *e.g.* polyelectrolytes of opposite charges within a so-called layer by layer assembly, [50]. The coating material surrounds the metallic part of the complex and the fluorescence substance is attached at its surface. In some cases, a coating, which is fluorescent by nature, such as a carbon shell, is used to stabilize the metallic part of the IBN complex, [101]. Moreover, a coating composed of mesoporous silica was suggested to enable the insertion of fluorescence substance within its inner pores, [97, 98]. In addition to a fluorescent compound, IBN can comprise a targeting agent and a chemotherapeutic drug such as folic acid and β-cyclodextrin, [102], providing additional functionalities to IBN but making this complex more difficult to fabricate under pharmaceutical standards. The distance between the fluorescent compound and the iron-based metallic part is often maintained sufficiently large to prevent fluorescence quenching and below a certain threshold to avoid the loss of the complex stability. When the fluorescent substance is an inorganic QD, it is possible to grow it directly on top of IBN external surface, and hence to avoid the presence of an organic coating, [72, 88, 54]. Finally, different types of super-structures have been proposed, which are composed of micelles, [103], filled or empty vesicles/spheres, [91, 74, 89, 86], matrix, [71], nanowires, [104], graphene oxide, [90], inside or at the surface which FIBN are inserted or

attached. Such super-structures maintain several FIBN complexes on or within the same support, hence providing a means to collectively send several FIBN towards a desired location, *e.g.* a tumor, hence possibly improving the targeting efficacy compared with a strategy relying on the movement of individual FIBN.

Most often, the FIBN complex is designed to prevent the release of the fluorescent compound and hence to ensure that the fluorescence remains stable as a function of time, *e.g.* by attaching the fluorescent compound (FC) by strong/covalent bonds to the coating of IBN metallic part, [102, 49, 61, 97, 63, 98, 79, 57, 65, 55, 68, 83, 32, 84, 105, 106], or by maintaining the FC inside the FIBN complex by encapsulating it inside a vesicle, [91). However, in one recent case, it was suggested to maintain a weak bond between FC and FIBN, [22, 23], to allow the operation of the probe through the release of FC from the FIBN complex, hence yielding an increase of the fluorescence intensity of FC through a de-quenching mechanism, *i.e.* the fluorescence of FC is initially quenched when FC is attached to FIBN and is then de-quenched when FC is released from FIBN, [22, 23]. This method was conceived to yield enhanced sensitivity, due its operating conditions relying on the detection of fluorescence increase instead of constant fluorescence. In addition, it can detect the release of a fluorescent anti-cancerous drug, *e.g.* Doxorubicin, paclitaxel, or bleomycin, [107], hence possibly enabling the monitoring of chemotherapeutic drug activity when the latter is triggered upon release of the drug from FIBN.

Several types of FIBN are commercially available, at prices that differ depending on the product between ~7 and ~300 euros per mg of FIBN. FIBN are available in the following different configurations : i) dyes are covalently bound to FIBN, eventually coated with dextran/hyroxyl-starch, *i.e.* Absolute Mag from CD, Magdye from Ocean Nanotech, nanomag®-CLD-redF and synomag®-CLD-far redF from Micromod, MP25/350-FC/RB/Cy3/Cy5/Cy5.5 from NANOCS, ii) dyes are sandwiched between a magnetic core and a polysaccharide matrix, *i.e.* nano-screen MAG (affinity) from Chemicell, iii) dyes are comprised in a polystyrene/silica matrix surrounding FIBN magnetic core, *i.e*. SPHERO™ Carboxyl Fluorescent Magnetic Particles from Spherotech, iv) dyes are weakly bound to magnetosome surface and

could be released from this surface under the application of a stimulus to yield an increase in fluorescence intensity (table 1).

III. DETECTION METHODS OF NON-FLUORESCENT IRON-BASED NANOMATERIALS

Dark-field optical microscopy (DFM), is a relatively cheap/simple method that can image IBN down to single IBN resolution, using a microscope shining light, *e.g.* white one, on IBN with the help of a condenser to ensure accurate light focusing, and the scattered light then travels through an objective lens before being observed/recorded. In DFM, the light scattered by IBN is recorded at localized surface plasmon resonance (LSPR) wavelength, *e.g.* using a spectrometer connected to a CCD camera, [108]. DFM relies on Rayleigh scattering by IBN, which occurs under conditions where the wavelength of the incident light beam is large compared with IBN sizes resulting in elastic interactions between this beam and IBN and in an absence of energy loss. This method can be used to visualize an assembly of IBN through an image built from the intensity of light scattered by this assembly after removal of un-scattered light. The region, which surrounds IBN and where scattering does not occur in the absence of a scattering object should appear dark in the image, shedding light on the name *''dark-field microscopy''*. To reach a high scattering efficacy, a material with strong surface plasmonic resonance, *i.e.* essentially gold, can be added at the surface of IBN, [101]. Hence, nanoparticle complexes made of Au nano-seeds organized at IBN surface were brought into the presence of human fibroblast cells. It was possible to observe assemblies of these IBN in these cells using a dark-field microscope, apparently with a better resolution than the bright field microscope although this aspect was not discussed in this study, [109].

Near Field Scanning Optical Microscopy (NSOM) uses laser light that travels through an aperture with a diameter smaller than the laser wavelength to create an evanescent field, which then excites and images IBN down to individual IBN level. NSOM presents the double advantage of reaching very high resolution down to 10 nm, [110], which is well below the diffraction limit of $\lambda/2$ estimated for an objective with numerical aperture of 1, and of enabling to extract topographical information of the measured sample

when NSOM is combined with atomic force microscopy (AMF). NSOM microscopes usually consist of a laser light beam, which travels through an optical fiber, whose ending part, which serves to illuminate IBN and to collect the scattered light, *i.e.* the so-called scanning tip, is coated with a metal, pulled or stretched. The laser light beam further crosses a polarizer and a beam splitter to remove light not interacting with FIBN from the scattered light. The scattered signal is further detected by standard optical detectors, such as avalanche photodiode, photomultiplier tube (PMT) or CCD camera. A so-called feed-back mechanism can be used to achieve high resolution images without artifacts. Thus, it was demonstrated that IBN internalized in MCF7 breast cancer cells could be visualized by NSOM, giving rise to dark spots in transmission NSOM images, resulting from IBN light absorption at 488 nm. Furthermore, AFM images, which displayed the geography of the cell surface through which IBN were engulfed, were also provided as sisters images of NSOM images, [111].

Raman spectroscopy (RS) is another method, whose principle relies on inelastic light scattering by a nanomaterial notably following light energy absorption through lattice vibration of this material. It consists in recording a Raman Spectrum, whose peaks positions and intensities depend on the composition/structure of the studied material, further highlighting its presence or absence. Raman phenomena can be triggered by several different laser sources operating within a wide range of different wavelengths, *i.e.* typically between 488 nm (Argon laser) and 1064 nm (Nd:YAG laser), where a tradeoff between long wavelengths resulting in the most efficient tissue/cell penetration and low wavelength yielding the strongest Raman signal, which is proportional to $1/\lambda^4$, should be determined, [112]. A Raman microscope typically contains a laser for IBN excitation, filters to remove laser light not interacting with IBN, a spectrometer or monochromator for scanning the different wavelengths of the scattered light, and standard detectors for measuring the strength of the scattered light. It measures so-called Raman Shifts, resulting from the light scattered by IBN, and operates either in standard or hyperspectral mode, where it detects wavenumber(s) associated with one or several type(s) of IBN, further providing images determining IBN location. Carrying out RS in the presence of IBN covered by a plasmonic material such

as gold, leads to surface enhanced Raman spectroscopy (SERS) effect, *i.e.* an amplification of the Raman signal due to plasmonic resonance at NP surface. Without such mechanism, it may be difficult to record a Raman spectrum with good resolution/sensitivity. By using various SERS based IBN, ultrasensitive detection of various cancer biomarkers could be reached, *e.g.* Fe_3O_4@Ag NP associated with DNA detected miRNA let-7b down to 0.3 fM, [113], SPION-PEI associated with Au NP and Folic Acid enabled the detection of a single HeLa cell per mL of collected blood, [114], while a sandwiched type immunoassay, consisting of Fe_3O_4 IONP coated by a silica shell attached to antibodies capturing tumor exosomes enabled to reach rapid detection, *i.e.* within 2 hours, of tumor exosomes via a SERS signal, [115].

IV. DETECTION METHODS OF FLUORESCENT IRON-BASED NANOMATERIALS

The methods described in the previous section, which don't necessitate the presence of a fluorescent compound associated with IBN, can be of insufficient resolution to observe individual or weakly concentrated IBN. Thus, to improve the signal quality, visible/infra-red light detection methods have been developed in which FIBN are excited by an incident light beam, resulting in light emission used for reconstituting a fluorescence image. The description of the different existing types of fluorescent microscopy (FM) are reviewed elsewhere, [116]. With FIBN, certain drawbacks of FM can be overcome such as fluorophore photobleaching [117], weak dye quantum yield [118], and a narrow absorption band of many fluorescent compounds, (FC), [119]. Indeed, FIBN enable the attachment of several FC to a single FIBN hence increasing their concentration, a strong absorption in particular below 500 nm, the adjustment of fluorescence mechanisms through the design of the nanoparticulate complex, which can result in the presence or absence of electron transfer between the crystalized part of FIBN and the fluorescent compound and in FC being associated to the FIBN complex by weak or strong bonds, depending on whether or not the release of FC is desired.

Wide field epifluorescence microscopy (WFEM) is the easiest fluorescent imaging method. Following laser light illumination, it yields a fluorescent image of FIBN, which is a superposition of images obtained at all different focal planes. WFEM contrasts with confocal microscopic images, where fluorescence originates from a specific focal plane. WFEM loses in resolution as the sample gets thicker and is best suited for thin sample with minimal autofluorescence, such as FIBN internalized in cells. It also requires the removal with adequate filters of laser light not originating from FIBN fluorescence. It can be combined with FIBN to yield efficient imaging at sub-cellular level, as has been shown for DMSA coated FIBN covalently attached to dyes, which produced membranous fluorescence when FIBN adsorbed on cell membrane and intracellular vesicular fluorescence when FIBN internalized inside cells, where these two distinct types of fluorescence could be achieved by varying FIBN incubation time and by deciding to apply (or not) a magnetic field, [49].

To further improve the detection of FIBN position within cells, confocal microscopy (CM) may be used. In CM, the combination of a microscope objective and a pinhole enables to focus a laser light beam on different focal planes localized at various depths of a sample containing FIBN, a method called optical sectioning. It yields a series of images from which a three-dimensional sample image can be reconstructed. In CM, the fluorescence originating from other planes than the focal one, is removed, hence resulting in a sharper and better resolved image with enhanced resolution compared with WFEM, *i.e.* typically 160-180 nm and 600 nm in lateral and vertical directions. Depending on FIBN sizes, on FIBN fluorescent properties, and on the optical quality of the used confocal microscope, such resolution could in principle allow the detection of a minimum of 1 to 100 FIBN. Using this method, it was clearly shown that fluorescent PVLA-coated FIBN were located inside hepatocyte cells and not at cell surface, [120]. Furthermore, CM, which is a widely used microscopy technique, enabled to distinguish the various blocks of a FIBN complex consisting of SPION (block 1), PEG (block 2), and antibody (block 3), where blocks 1, 2, and 3 appeared in black, green, and red, respectively, hence clearly showing the different locations of these blocks within the nanoparticulate complex, [52].

To reach a microscopic resolution below 200 nm, super-resolution light microscopy, (SRM), can be used, [121]. The term SRM encompasses a large number of different techniques, an example of which being structured illumination microscopy (SIM). SIM can reach a resolution of 100 nm in lateral directions by reconstructing an image, which is a superposition of images obtained for illuminations at different phases and angles. Due to its high resolution, SRM enables to obtain images in 3D of FIBN in interaction with cells, cell compartments or cell membrane, using different colors for labeling various entities at nanometer scale, [121]. To obtain highly contrasted images with this method, fluorescent CTDR and DAPI compounds were directly mixed with Hela cells, leading to beautiful images of the cell nucleus and its surrounding with IBN appearing in the reflectance mode as white dots localized inside (blue) and around (red) cell nucleus, [122].

Fluorescence resonance energy transfer (FRET) relies on the detection of the variation of fluorescence of a donor induced by the appearance or disappearance of a transfer of electrons between so-called donors and acceptors in close proximity, *i.e.* typically separated by less than 10 nm. To carry out optimal FRET measurements, specific properties are required both for the microscope used for imaging and for the FRET pair. On the one hand, most inverted microscopes could in principle be used for FRET microscopy, provided that they include a camera, which is sensitive enough to detect the fluorescence signal of FIBN, *e.g.* a high-resolution CCD camera, as well as interference filters allowing to block the light not arising from the fluorescence signal of FIBN. On the other hand, the FRET pair contained in FIBN should be characterized by: i) a well-adjusted ratio between the concentration of donors and acceptors, ii) an absence of photobleaching, iii) a sufficient overlap between donor fluorescence emission and acceptor absorption, iv) a minimal overlap between donor absorption and donor emission, v) no excitation of acceptor at donor excitation wavelength, v) a sufficiently long donor lifetime, and vi) a low donor polarization anisotropy. Most interestingly, these properties can be optimized in FIBN, *e.g.* by accurately selecting the FC, by adjusting the distance between the FC and IBN magnetic core through a tuning of the coating thickness, by controlling the number/position of FC bound to IBN magnetic core. In most FRET studies, a FRET-

based IBN complex was activated through the binding of FC to IBN or via the structural change of the FRET IBN complex, which took place without FC release from IBN. FIBN can contain FRET pairs consisting of a donor such as GFP, [123], Carbon dots, [124], FITC, [125], PFR, [126], and an acceptor such as CdTe QD, [123], Au [124, 126], or iron oxide nanoparticle (IONP), [125]. When FC gets linked to IBN to form a FRET IBN complex, it yields a fluorescence decrease of the FC donor and the binding of FC to this complex can then be detected. Hence, FRET can be used to detect the binding of a substance of interest such as sarcosine, [123], histamine, [124], thiol, [126], to IBN with a high sensitivity, *i.e.* typically in the nM range, [123], resulting in a highly sensitive diagnostic test. FRET can also serve to monitor the release of a cancer drug such as platinum (IV), following the action of an enzyme triggering such mechanism in the presence of FITC whose fluorescence changes are measured with FITC detachment from IBN, [125].

Although microscopic techniques often allow to obtain well-resolved images, they can hardly monitor very localized phenomena at the nanometer scale and suffer from the dependence of the fluorescence intensity on tissue light absorption/scattering. To overcome this hurdle, fluorescence lifetime imaging (FLIM) was developed. FLIM provides microscopic images, in which each pixel intensity is determined by the fluorescent decay rate (FDR) of the material that it contains, hence allowing to clearly differentiate between materials of different FDR through a contrast in the FLIM image. FLIM could be used to detect FIBN associated with photosensitizers inside tumor cells or FIBN internalized in tumors. It could also provide a method for FRET measurement described above, which does not rely on fluorescence intensity but on fluorescence lifetime, hence making FRET outcome potentially less dependent on tissular environment. FLIM measurements on FIBN consisting of an iron oxide core coated by polymers bound covalently via imine bonds to DOX and incubated (or not) with MCF-7 breast / H1299 lung cancer cells showed that DOX lifetime was lower for incubated FIBN complexes, *i.e.* ~1 ns, than for non-incubated FIBN complexes, *i.e.* ~4.6 ns. Such behavior may be attributed to DOX release from FIBN complexes under acidic intracellular pH, [127].

Fluorescence anisotropy (FA) is a light detection method, which measures fluorescence anisotropy, *i.e.* the intensity of fluorescence for different light emission directions. Its mechanism is based on the existence of photon polarization in light emitted by a FC when the exciting photons are polarized in a specific direction. Hence, a microscope used for FA measurements contains polarizers to polarize the light illuminating FIBN and to record the strength of the fluorescence intensity signal as a function of the light polarization direction. FA further relies on the principle that a molecule leads to less FA when it is in movement than when it is immobilized, since a molecule can more easily emit light in all directions when it is free to rotate than when it is fixed. Thus, this method was first used to measure the melting temperature of the membrane of a liposome containing IONP, by making such membrane fluorescent and by measuring FA as a function of increasing temperature under alternating magnetic field application, [128]. It could also be employed to determine the heating mechanism of IBN during magnetic hyperthermia. For example, IBN encapsulated in a silica matrix were shown to heat through a dominating Néèl contribution [129].

Two-photon microscopy (TPM) usually requires the use of a fluorescence microscope containing a laser of sufficiently large power, *e.g.* a femtosecond pulsed laser, with typical emission in the near infrared. It has been developed to image FIBN in regions that are inaccessible/too deep for the microscopy methods described above. Its principle relies on the use of an excitation light source with a wavelength that is twice that of single photon excitation (SPE). Two-photon excitation (TPE) presents the advantage of limiting tissue light scattering due to the use of long wavelengths, thus making it possible to image tissues at a certain penetration depth, *i.e.* typically 1 mm compared with only a few micrometers for single photon microscopy. The power required for TPE is however much larger than for SPE, requiring the use of a pulsed laser, since the number of photons reaching the region to be imaged should be sufficiently large so that the probability for the energies of two photons of energies E/2 to be simultaneously absorbed by the FC and result in its excitation, should be sufficiently large for fluorescence excitation to occur. As an example, FeS QD conjugated with HER2 antibodies were injected intravenously in mice bearing MCF7

subcutaneous tumors, and their presence in the tumor was revealed by TPE at 800 nm at a depth of up to 500 µm by a cyan color due to FeS QD fluorescence, [130]. Some FIBN such as FePt NP associated with NOPS fluorescent dye, which are non-fluorescent under SPE due to fluorescence quenching, can be made fluorescent under TPE and used for *in vivo* imaging, *e.g.* to image the mouse neocortex, [131]. Interestingly, it was suggested that TPE efficacy could be optimized, not necessarily by choosing an adapted dye that is incorporated in FIBN, which is always a complex thing to do, specially to reach a good FIBN stability, but by tailoring the surface of FIBN to make this material a strong absorber of NIR-IR light, as demonstrated for Fe_3O_4 NP with a surface modified by trimesic acid (TMA) [132].

To follow the fate of FIBN in an organism, fluorescence tomography (FT) can be used. In FT, the body part of a small animal (rat, mouse) in which FIBN are located is trans-illuminated with an IR/NIR laser. The fluorescent light transmitted through the animal is then detected after removal of the excitation signal not due to fluorescence, hence enabling to reconstruct a 2D or 3D fluorescence image (depending on FT apparatus) of a body part (BP) containing FIBN by gathering the fluorescence of different portions of the BP recorded at different angles. In this case, fluorescence is generated by a fluorescence compound associated to FIBN, *e.g.* Cy5.5 or NIR emitting semiconducting polymer with excitation/emission wavelengths of 670/695 nm, [133], or 360/660 nm, [134], respectively. Thus, when FIBN associated with specific targeting agents such as anti-EGFR, [135] or folic acid, [134] were administered intravenously to mice, they specifically targeted MDA-MB-231 breast and A549 lung subcutaneous tumors, [133, 134], reaching maximum FIBN tumor accumulation at 6 and 36 hours following FIBN administration, as revealed by the strongest fluorescent signal observed at these time points, [133, 134].

IV. FLUORESCENT IRON OXIDE NANOPARTICLES FOR DETECTING TUMOR MICRO-ENVIRONMENT

The tumor micro-environment consists of a wide range of different molecules, cells, or entities contained in tumor, such as angiogenic blood vessels, immune cells or fibroblasts, various signaling molecules, or the extracellular matrix. Its detection is important to yield accurate tumor diagnosis. In an interesting

study, a probe was fabricated to detect metalloprotease-9 (MMP-9), which are known to be activated in TME. Such probe consisted of Fe_3O_4 NP linked to a Cy5.5 through a bond that was cleaved in the presence of MMP-9, thus suppressing the FRET mechanism between the NP and Cy5.5. In other words, this probe indirectly enabled to detect the TME by highlighting the loss of FRET, a method that was then elegantly applied for the detection of colon cancer, [136].

V. RECENT INNOVATIONS OF LIGHT INTERACTING IRON-BASED NANOMATERIALS IN ONCOLOGY

In addition to the fluorescent probes already described, which operate through a fluorescence de-quenching mechanism, [22, 23], and studies which are in line with or complement older works, [137-147], some recent papers in the field of FIBN have brought to light some remarkable innovations. First, radio-luminescent FIBN produce a luminescence intensity proportional to the x-ray dose at which they are exposed. They could therefore potentially be used to monitor the doses of X-rays administered to a cancer patient, [148]. Secondly, an original detection system for cathepsin L was described. It operates by detecting the fluorescence quenching caused by the aggregation of FIBN associated with polymer dots in the presence of cathepsin, [149]. Thirdly, IBN associated with thermo-responsive fluorescent polymer (TFP) which can release DOX in response to temperature changes, were shown to be taken up by prostate/skin tumor, resulting in tumor fluorescence that could serve for their detection. Furthermore, DOX release led to efficient tumor cell destruction at 41 °C. Hence, such nano-systems displayed a controlled drug release mechanism, which could be monitored by fluorescence, [150]. The presence of a fluorescence probe in ION was also shown to enable the detection of the specific tumor targeting of these NP or their internalization in tumor cells, using a variety of different types of FIBN, [151].

VI. TOWARDS CLINICAL APPLICATIONS OF VISIBLE AND INFRA-RED LIGHT DETECTION METHODS COMBINED WITH IRON-BASED NANOMATERIALS:

Early cancer detection, which is needed to yield efficient cancer prognosis, relies on certain detection methods, which could be made more sensitive by using FIBN. First, liquid biopsy (LB), which consists

in an analysis of certain blood components such as circulating tumor cells (CTC) and extracellular vesicles, has a strong cancer predictive power, since it can in principle highlight at the same time cancer occurrence, cancer heterogeneity, and cancer evolution, as demonstrated for lung, colorectal, prostate, melanoma, breast and pancreatic cancers, [152, 153]. In addition, it is less invasive than tissue biopsy. LB can be carried out using an apparatus that detects and identifies by fluorescence the presence of extracellular vesicles. It has been shown that FIBN consisting of fluorescent magnetic mesoporous silica nanoparticles conjugated to the antibody of epithelial cell adhesion molecule (EpCAM) could enable to isolate and then detect CTC, hence demonstrating its utility in LB, [154]. Second, a system of detection of superficial tumors such as those of the skin, typically consisting in a fiber optic–based fluorimeter, [155], could yield improved efficacy in the presence of FIBN, as demonstrated when SPION covalently conjugated to anti-cancer drug Epirubicin (EPI) with red fluorescence properties were shown to cross the derma under magnetic field application, enter and destroy skin WM266-4 metastatic human melanoma cells, as well as specifically release EPI through a pH dependent release mechanism, which takes advantage of the acidic tumor microenvironment, [34]. Third, fluorescent endoscopy could be carried on various cancers, *e.g.* gastrointestinal, [156], pancreatic, [157], gastric/stomach, [158], esophageal, [159], or kidney, [160] cancers. Combining standard endoscopic fluorescent apparatus with FIBN associated to a targeting moiety (amino-terminal fragment) could improve the quality of the fluorescence signal due to the specific tumor targeting and imaging of FIBN, [157]. In the same spirit, it was shown that the position of FIBN encapsulated in a hydrogel with upconverting materials could be adjusted via magnetic targeting to enable the fluorescent compound of FIBN to reach the desired target, hence resulting in an improved endoscopic image, [161]. Fourth, colonoscopy, which is a similar method than endoscopy but specifically targets colon tumors and requires the patients to follow a specific preparatory treatment before imaging to clear out the colon, *i.e.* by drinking cleansing solutions/laxatives/enemas and by observing a diet. Among the innovations in this field, it is worth mentioning a colonoscopy imaging endoscopic system that eliminates tissue autofluorescence and can distinguish between FIBN with different absorption/fluorescent properties. It combines a cysto-urethroscope, a multi-spectral imaging system, a

CCD camera, a Xenon lamp, as well as lenses/optical fibers to carry the exciting/emitted light between the apparatus and colon tumor, [162]. Furthermore, using FIBN during colonoscopy can yield a reduction in dye photobleaching as well as the specific imaging of colon tumors when FIBN are bound to a tumor-targeting ligand such as peanut agglutinin and anti-carcinoembryonic antigen antibodies (αCEA), [163].

One of the main interests of using FIBN in combination with optical methods resides in the faculty of these nanomaterials to specifically target tumors, hence enabling to improve tumor detection/treatment. Passive targeting, *i.e.* via the well-known enhanced permeability and retention effect (EPR), [164], is the most common employed strategy. Its efficacy seems to depend on the nature of the body part. On the one hand, it was shown that FIBN associated with pH-activatable NIR dyes could accumulate in 4T1 tumors three hours after their injection and trigger a fluorescence signal in these tumors due to their acid environment, which persisted for 24 hours, [165]. On the other hand, when tumors are poorly vascularized, the EPR effect is not pronounced. This is the case for SKOV3 tumors, where other methods than passive targeting, *e.g.* magnetic targeting, need to be used to reach FIBN tumor accumulation, [167]. Targeting could also be achieved by using FIBN associated with a molecule that targets the region of interest, as was shown first for fluorescent iron oxide-carbon hybrid nanomaterials conjugated with CD44 monoclonal antibodies that specifically reach 4T1 breast cancer cells, yielding fluorescence of these cells, [167], second for FIBN associated with a protein targeting riboflavin, which is overexpressed/activated in cancer/endothelial cells, and a fluorescent moiety (flavin mononucleotide), demonstrating efficient fluorescence of PC-3, DU-145, LnCap cancer cells and activated HUVEC endothelial cells, [15], third for FIBN associated with fluorescent dye and folic acid that target KB cancer cells as demonstrated in vitro through fluorescence experiments, [168]. The targeting molecules incorporated in IBN and their associated cellular targets form pairs, whose list is provided elsewhere, [169, 170]. The presence of iron in FIBN makes these materials sensitive to the application of an external magnetic field. Thus, it was shown that FIBN administered intravenously to GBM bearing mice could be magnetically retained in tumor neovasculature and surrounding tumor tissues, using a magnetic field applied on the tumor via a

micromesh, (56). Interestingly, it was shown that FIBN could be captured by certain cells carrying FIBN to a location that needs to be imaged. For example, when FIBN were associated with ICG and injected intravenously to rats suffering from cerebral aneurysms (CAs), they were captured by macrophages that transported the nanoparticulate complex to CAs, hence providing a means to image CAs, [171]. It can be taken advantage of the imaging capacity of FIBN to efficiently deliver a molecule of therapeutic interest, *e.g.* FIBN surrounded by a mesoporous silica shell containing siRNA were efficiently carried to Hela cells under magnetic guidance and visualized by FI [172].

Most interestingly, FIBN can also be used in the context of cancer treatments. First, the well-established and valuable method of fluorescence guided surgery (FGS), which is most commonly used on brain tumors to improve tumor resection, avoid tumor re-growth, and prevent removal of healthy tissues, could benefit from the presence of FIBN. Practically, FGS operates under infra-red (IR) light illumination with relatively deep tissue penetration of 1-2 cm, [173]. Hence, it can serve to excite/detect FIBN that can be made fully operational in the IR range of wavelengths. As an example, FIBN associated with DiI were used to label certain microglial BV2 cells, resulting in FIBN efficiently crossing the BBB and then imaging by fluorescence tumor border demarcation for a prolonged period of 4 to 24 h following FIBN administration through the carotid artery in an orthotopic glioblastoma mouse model. In this case, FIBN also led to an inhibition of M2 markers (arginase-1 and CD206), possibly reducing immunosuppressive effects induced by M2-like phenotype of microglial cells, [174]. Compared to other types of NIR nanoparticulate fluorescent materials foreseen for this application, such as carbon dots, CuInSe QD, cornell dots, Up-converting NP, aggregation-induced emission NP, FIBN present the advantage of being bio-compatible and orientable through the application of an external magnetic field, [175]. Second, FIBN could be heated via a method called photothermal therapy (PTT), and trigger heat-induced anti-tumor activity, [176]. Thus, FIBN conjugated with certain dyes (MHI-148) were injected in subcutaneous SCC7 mouse tumors and heated during 10 minutes at a maximum temperature of 50 °C under the application of a 808 nm laser of 1 W/cm^2, resulting in full tumor disappearance after 8 days, [177]. Furthermore, it is

possible to combine PTT with fluorescence imaging (FI) to determine FIBN localization. For example, FIBN made of an assembly of iron oxide and carbon NP associated with fluorescent ICG enabled reaching ICG photostability and efficient long-term FI and PTT capability, *i.e.* intravenous injection of these FIBN on mice bearing 4T1 subcutaneous tumors followed by tumor illumination at 808 nm and 2 W/cm^2 for 5 minutes led to tumor temperature elevation up to a maximum temperature of 47 °C and to full tumor disappearance. Interestingly, the fate of FIBN after its injection in mouse organism could be followed by FI excited at 704 nm using an ex in vivo imaging system. FI nicely helped determining the lapse of time following FIBN injection that yielded maximal FIBN tumor accumulation, *i.e.* 8-10 hours, [178]. The practical application of PTT combined with IF can be made even more efficient by incorporating in FIBN a fluorescent compound with adjustable emission/excitation wavelengths and a releasable chemotherapeutic drug, as demonstrated for FIBN associated with carbon dots and DOX that yielded efficient imaging and destruction of mouse melanoma B16F10 cells through a synergy between chemotherapeutic and heating anti-tumor activity, [96]. The use of IBN with PTT further enables NP concentration at tumor cell location via the application of a magnetic field, as highlighted for IBN incorporated in PLA microcapsules functionalized with graphene oxide that were heated by a 808 nm laser of 2 W/cm^2 during 10 minutes in the presence of Hella cancer cells, resulting in more efficient cancer cell destruction in the presence than in the absence of magnetic field application for optimal IBN concentration of 0.5 and 1 mg/mL, [179]. Third, Photodynamic therapy (PDT) is another modality of cancer treatment that can be implemented using iron-based nanomaterials associated with a photosensitizer (IBN-PS), which trigger anti-tumor activity via singlet oxygen generation under infra-red light excitation, and is currently in use in the clinic to treat several cancers, [180]. IBN-PS was reported to yield better PS solubility and more efficient tumor targeting compared with free PS, hence improving PDT efficacy. The latter has been demonstrated, first for mice bearing 4T1 tumors injected intravenously with Ce6-FIBN followed by tumor light exposure at 650 nm and 75 mW/cm^2 during 30 minutes, [181], second for mice with A539 xenograft tumors receiving intravenously IBN conjugated with thiolated heparin–pheophorbide, which is a PS designated to be specifically activated at tumor site, followed by

several 30 minutes laser applications at 670 nm and 4 mW/cm^2, [179], third for mice having subcutaneous gastric cancer tumors administered intravenously with FIBN associated with Ce-6, for which the combination of FI and PDT was reported under similar laser excitation conditions at 630 and 633 nm, enabling to monitor FIBN tumor localization before, during, and after tumor treatment, [181]. These three treatments led to tumor growth retardation, but not to full tumor disappearance. Figure 3 summarizes the various applications of light-interacting iron-based nanomaterials.

CONCLUSION

The detection and treatment of cancer are major public health issues. These two concepts are closely linked to each other, *i.e.* in general the earlier or the more precisely a cancer is detected in the body, the greater the chances of treating it effectively. Based on this observation, it appears interesting to develop methods that can improve detection and treatment of tumors through local approaches. When combined with various optical methods, iron-based nanomaterials achieve this double objective. Indeed, they are biocompatible and can target tumors by various mechanisms, *i.e.* passive, active, and magnetic targeting, [183-186]. When they are covered with a plasmonic material, such as gold or silver, the light diffusion that they generate under the effect of a radiation makes it possible to detect tumor cells, which contain them, in particular with the help of dark field, Raman or near-field scanning optical microscopy. A more important number of applications can be foreseen when IBN are combined with a fluorescent compound. For example, tumor cells, which are made fluorescent by the presence of FIBN, can be detected with wide-field epi-fluorescence microscopy. The sensitivity of the detection can further be improved by using confocal or super-resolution microscopy. Moreover, dynamic phenomena such as FIBN diffusion can be monitored by various microscopic methods, which measure the variation as a function of time and FIBN location of certain fluorescence parameters such as fluorescence lifetime, intensity, or anisotropy, using FRET, FLIM or FA microscopy. A method has also recently been developed to detect the release of a fluorescent drug from iron-based nanoparticles by monitoring a dequenching mechanism, *i.e.* the fluorescence of FIBN is initially quenched in the absence of excitation/perturbation and then de-quenched

after FC release. TF imaging is another microscopy tool for imaging FIBN at a certain tissular depth, hence providing a tool to detect non-superficial tumors. Finally, although this method is currently reserved to small animals (rats, mice), fluorescence tomography can be used to visualize FIBN within the whole organism, thus making it possible to follow FIBN trajectory inside/outside a tumor. In combination with these various optical methods, FIBN can be used in liquid biopsy to improve the detection in blood of certain cancer biomarkers, they can serve to detect superficial tumors, *e.g.* those of the skin, or to improve the resolution of fluorescence imaging in endoscopic/colonoscopic tumor tissue examination. FIBN can also be employed in the context of cancer treatment, where they can guide the surgeon by illuminating tumor edges, and thus potentially allow him to increase the size of the tumor portion that he can remove at tumor margin. FIBN can directly destroy the tumor, either through heat, *i.e.* when FIBN are exposed to a laser beam of suitable wavelength and sufficient power to produce a temperature increase via PTT, or by generating singlet oxygen, *i.e.* when FIBN are associated with a photosensitizer and exposed to a laser beam to yield PDT. As a whole, iron-based nanomaterials appear to be very interesting and promising materials to fight cancers when they are combined with various optical methods to yield early cancer detection and localized tumor treatment.

FIGURES AND TABLE:

Figure 1: A schematic diagram showing examples of fluorescent iron-based nanomaterials (FIBN). In a first category, the fluorescent compound (FC) is either attached to the NP magnetic core, embedded in a matrix (mesoporous or not) embedding the NP magnetic sore, or sandwiched between an external layer and the NP magnetic core. In a second category, FC is weakly bound to the NP magnetic core. In the first case, FC is sufficiently strongly associated to the NP magnetic core to prevent its dissociation and the fluorescence intensity of FC remains stable over time. In the second case, the weak interaction between FC and the NP magnetic core enables FC dissociation under various physico-chemical disturbance, such as pH, temperature variation or the application of a radiation, yielding a de-quenching mechanism and an increase of the fluorescence intensity.

Figure 2: The different methods of light interaction with iron-based nanomaterials as a function of wavelengths. Only optical methods operating in the infrared and visible regions through a scattering/fluorescent mechanism are covered in this review.

Figure 3: Various applications of light-interacting iron-based nanomaterials for cancer treatment and detection.

Table 1: For various FIBN described in the literature, magnetic composition, type of fluorescence substance that it contains, size, magnetization, coercivity, stability, type of complex that it is made of, fluorescent properties, and various applications.

no detachment of fluorescent tag
detachment of fluorescent tag
The different types of magneto-fluorescent iron oxide nanoparticles
Fluorescence quenched
Fluorescence activated
Fluorescent tag covalently bound to NP coating
(a)
coating
Magnetic core
Fluorescent tag embedded in surrounding matrix
(b)
Magnetic core
Surrounding matrix
(c)
Fluorescent tag sandwiched between layer and magnetic core
Magnetic core
layer
Physico-chemical disturbance (pH variation; radiation)
Fluorescence activated under dissociation
Weak binding
(d)
Magnetic core
coating
Fluorescent tag weakly bound to NP coating

Figure 1

Methods of light interaction with iron-based nanomaterials at different wavelengths

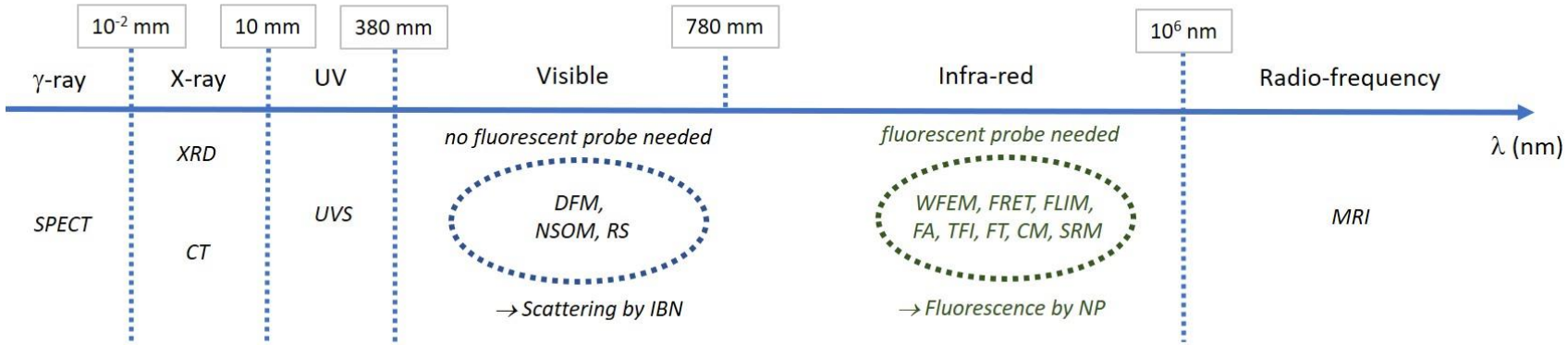

CM: Confocal microscopy**; CT:** Computing tomography; **DFM:** Dark field microscopy; **FA:** Fluorescence anisotropy; **FLIM:** Fluorescence lifetime imaging microscopy **FT:** Fluorescence tomography; **FRET:** Fluorescence resonance energy transfer; **FTIR:** Fourrier transform infra-red absorption/transmission; **TFI:** Two-photon imaging; **NSOM:** Near field scattering optical microscopy; **RS :** Raman scattering (infra-red range); **SPECT:** Single-photon emission computed tomography; **SRM:** Super-resolution microscopy; **UVS:** UV absorption spectroscopy; **WFEM:** Wide field epifluorescence microscopy;

Figure 2

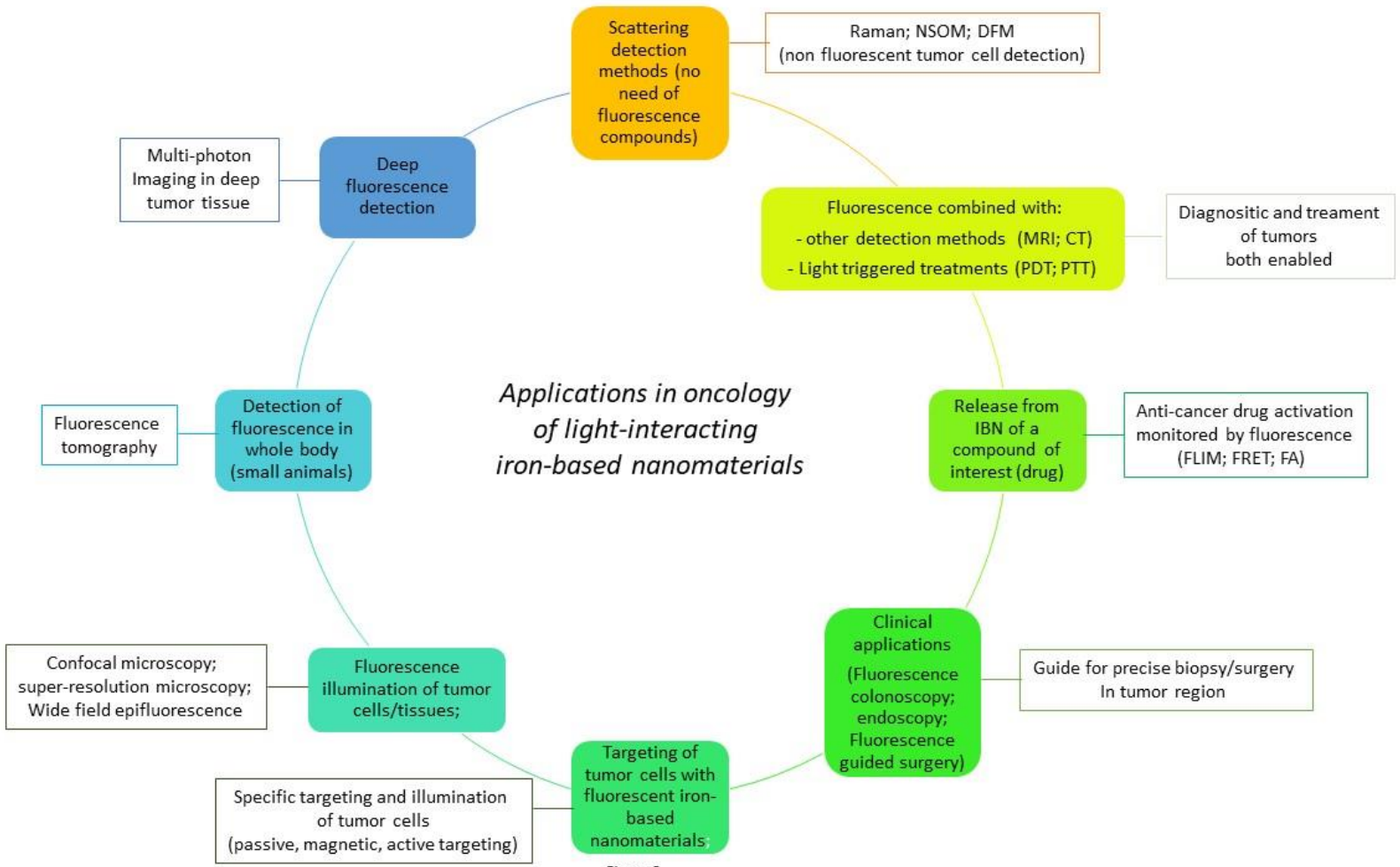
Applications in oncology of light-interacting iron-based nanomaterials
Scattering detection methods (no need of fluorescence compounds)
Raman; NSOM; DFM (non fluorescent tumor cell detection)
Fluorescence combined with:
- other detection methods (MRI; CT)
- Light triggered treatments (PDT; PTT)
Diagnositic and treament of tumors both enabled
Release from IBN of a compound of interest (drug)
Anti-cancer drug activation monitored by fluorescence (FLIM; FRET; FA)
Clinical applications (Fluorescence colonoscopy; endoscopy; Fluorescence guided surgery)
Guide for precise biopsy/surgery In tumor region
Targeting of tumor cells with fluorescent iron-based nanomaterials
Specific targeting and illumination of tumor cells (passive, magnetic, active targeting)
Fluorescence illumination of tumor cells/tissues;
Confocal microscopy; super-resolution microscopy; Wide field epifluorescence
Detection of fluorescence in whole body (small animals)
Fluorescence tomography
Deep fluorescence detection
Multi-photon Imaging in deep tumor tissue

Figure 3

Magnetic composition	Fluorescent substance	Size (nm)	Magnetization (MS) Coercivity (HC)	Stable (max conc.)	Type of complex containing magnetic/fluorescent substances	Fluorescent property and application	Ref	Commercialization
Magnetite	FITC	125 (HD)	NA	Yes (NA)	IONP coated by SiO_2 shell attached to FITC + folic acid + β-cyclodextrin (covalent)	Abs max: 490 nm ; em max: 515 nm → Cell imaging	102	NA
Maghemite	RhB fluorescein diacetate maleimide	30 (HD)	Ms = 8 emu/g Hc = 0 Oe	Yes (NA)	IONP coated by DMSA attached to RhB or fluorescein derivative (covalent)	Abs max: 490 nm ; em max: 516 nm (RhB) Abs max: 555 nm; em max: 578 nm (Fluo) (λ shift between free/conjugated dyes < 5 nm) → Cell membrane imaging (wo B) → Chains of magnetic endosomes (wB)	49	NA
$CoFe_2O_4$–Cr_2O_3 NP	None	30 (D)	MS = 5 emu/g Hc = 482 Oe	Yes (NA)	NP coated with SiO_2	Abs max : 260 and 360 nm ; em max: 460 nm → Cell imaging	95	NA
Maghemite	FITC	9 (HD)	NA	Yes (NA)	IONP coated with SiO_2 or carboxy-methyl-chitosan attached to FITC (covalent)	Abs: 495 nm; em max: 516 nm (no λ shift between free/conjugtaed FITC) → Cell labelling (fluorescence + MRI)	61	NA
Magnetite	polymethacrylic acid (PMA)	280 (D)	MS = 30-60 emu/g	NA	IONP coated with mesoporous SiO_2 + binding of PMA on SiO2 (covalent)	→ Cell labelling (fluorescence + MRI) →Dox within silica pores can be released inside cells → FA for tumor cell targeting	97	NA
Magnetite	QD (CdSe/CdS)	9 (QD) 6 (IONP)	Ms = 15 emu/g	Yes (NA)	Assembly of IONP surrouned by sylica layer containing QD + PEG (outer surface)	Visualization of NP at location of mouse brain metastases after NP iv injection → ⇓ quantum yield compared to free QD (abs by ION) → ⇓ M_s compared with free IONP	70	NA
Magnetite	silane modified fluorescent organic dye (RITC)	60 (D)	NA	NA	Fe_3O_4 covered by SiO_2 shell conjugated with cetuximab; RITC contained in SiO_2	Em max = 555 nm NP accumulate in mouse colon cancer (visualisation by MRI and fluorescence); ↑ NP accumulation when magnetic field applied on tumor site	52	NA
Magnetite	QD [Qdot 655 ITK amino (PEG), Invitrogen Corp)	150 (D)	NA	NA	Fe_3O_4 NP embedded in polystyrene matrix coated with QD embedded in PLGA + PTX	Abs/exc: 550-720 nm ; em: 630-790 nm → Fluorescence of ex vivo tumor tissues harvested after NP administration to mice (NP accumulate in tumors ; NP do not loose their fluorescence after circulation in mouse organism)	71	NA
Magnetite	CdSe QR; CdSe QD; CdSe@ZnS QD	35-45 (HD)	NA	NA	QD/QR grown directly on Fe_3O_4 NP. ZnS shell prevents release of toxic CdSe	Max Abs : 575 nm; Max em: 604 nm Quantum yield of IONP/CdSe@ZnS QD half quantum yield of CdSe@ZnS QD	72	NA
Magnetite	CdTe@ZnS QD	185 (D)	Ms = 37 emu/g Hc = Oe	Yes (NA)	Fe_3O_4 NP surface modified with carboxymethyl chitosan attached to QD + DOX with glutaraldehyde for covalent binding between different components	Abs = 365 nm; em = 560-580 nm Release of DOX from NP complex more important at pH 5 than pH 7 → ↑ lung A549 tumor cell toxicity	73	NA

D: Diameter (TEM measurement); HD: hydroduymaic diameter (light scattering measurement); NP: Nanoparticle; IONP: Iron oxide nanoparticle; FA: folic acid; wo B: without applicattion of magnetic field; W B: with application of magnetic field; abs: absorption; em: emission; QD: quantum dots

Table 1.1 *Properties of light interacting iron-based nanomaterials*

Magnetic composition	Fluorescent substance	Size (nm)	Magnetization (MS) Coercivity (HC)	Stable (time/ max conc.)	Type of complex containing magnetic/fluorescent substances	Fluorescent property and application	Ref	Commercialization
Magnetite NP	FITC	11 (D)	NA	Yes (NA)	amino acids (l-lysine and l-arginine) have been used as a linker and spacer between a fluorescent molecule (FITC) and a magnetic nanoparticle (Fe3O4)	Exc: 450 nm ; em = 500–570 nm	62	NA
Fe_2O_3/Fe_3O_4 NP	Cy5.5	97 (HD)	NA		NP core coated with siliceous shell attached to Cy5.5 + RGD (covalent) ; complex incorporated in micromesh	Red fluoresence → Magnetic micromesh apply magnetic fields that maintain NP in neovasulature	56	NA
Fe_3O_4 NP	Yb^{3+}/Er^{3+} or Yb^{3+}/Tm^{3+} co-doped $NaYF_4$	80 (D)	M_s = 38 emu/g (M_s = 80 emu/g for Fe_3O_4 NP)	NA	NP coated by layers of $nSiO_2$ + $mSiO_2$; $NaYF_4$: Yb^{3+}, Er^{3+}/Tm^{3+} + drug (IBU) inserted within the pores of slica + drug	Green emission (Yb^{3+}/Er^{3+}) ; Blue emission (Yb^{3+}/Tm^{3+}); excitation at 980 nm (short λ emission after long λ excitation) → Release of drug / no release of fluorescent substance when NP in simulated body fluid	93	NA
Fe_3O_4 NP	RhB	NA	NA	Yes (two days)	NP coated by polyelectrolyte layer (LBL assembly) + RhB in contact with polyelectrolytes (interaction between positive RhB and negatvely charged polelectrolyte)	Em = 580 nm ; exc = 555 nm Quenching prevented by polyelectrolyte separating layer → Cellular imaging after internalization of NP (no cytotoxicity)	50	NA
Fe_3O_4 NP	CdSe QD	NA	Hc = 0 Oe	NA	Fe_3O_4 NP seeds to grow CdSe QD	Abs peak at 600 nm; em peak at 610 nm → Cellular imaging after internalization of NP (NP scattered in cells wo B; NP localized in one spot of cells w B)	88	NA
Fe_3O_4 NP	CdTe	70-80 (D)	MS = 6 emu/g Hc = 0 Oe	NA	CdTe–Fe_3O_4 / SiO_2 microspheres attached covalently to graphene oxide + DOX bound to graphene (hydrophobic interaction)	Exc = 400 nm; Em = 550 nm DOX released from complex (enhanced at acidic pH) → Cellular imaging after internalization of NP + NP cytotoxic towards HepG2 tumors following DOX internalization.	90	NA
Fe_3O_4 NP	CdTe NP	50-1000 (D vesicle) 2- 6 (D CdTe) 8 (D Fe_3O_4)	NA	NA	CdTe NP + Fe_3O_4 NP contained inside a hollow vesicle composed of polyelectrolyte	Exc 476 nm ; em in red → Alignment of vesicle in direction of applied magnetic field	91	NA
Fe_3O_4 NP	FITC	14 (D)	MS = 55 emu/g	Yes (months)	Fe_3O_4 NP coated with chitosan bound to FITC (covalent)	Exc = 488 nm ; Em = 520 nm → Cell labelling (efficacuy increases with inc time) → Coating reduces cytotoxicity → Suitable as MRI contrast agent	63	NA
Fe_3O_4 NP	CdTe NP	NP complex (D 120) 2 (D CdTe) 10 (D Fe_3O_4)	Ms = 1 emu/g (decrease in complex) Hc = 0 Oe	Yes	NP complex (filled vesicle): Fe_3O_4/CdTe NP embedded in mesoporous silica surrounded by shell of P(N-isopropylacrylamide)-graft-Chitosan microgels (PNIPAM-g-CS) + loading of Adriamycin (ADM) in vesicles	Abs peak at 480 nm; em peak at 530 nm → ADM release in vitro (↑ at a higher temperature and at lower pH). → ADM cytotoxic towards HepG2 cells. → NP complex visualized inside cells by fluorescence	74	NA
Fe_3O_4 NP	CdTe NP	34 (D)	Ms = 60 emu/g Hc = 0 Oe	Yes	Fe_3O_4 NP coated by several layers of polyelectrolytes attached to CdTe NP	Abs = 300-800 nm; em = 590-600 nm → Increase of the emission/absorbition intensity with the number of coating layers → NP can be moved with magnetic field	75	NA

Table 1.2

Magnetic comp.	Fluorescent substance	Size (nm)	Magnetization (MS) Coercivity (HC)	Stable (max conc.)	Type of complex containing magnetic/fluorescent substances	Fluorescent property and application	Ref	Commercialization
Magnetite	Atto 390; fluoroscein; Rh6G	100-400 (D)	Hc = Oe	Yes	hydrophobic fluorescent polymers + IONP incorporated in phospholipid micelles	Exc at 400-500 nm ; em at 450-600 nm → Manipulation by external magnetic field without loosing fluorescence properties → Enhanced contrast in MRI	60	NA
Fe_3O_4 NP	Ce6	20-30 (HD)	Ms = 50 emu/g	Yes	Fe_3O_4 coated with mesoporous silica shell bound to Ce6 (covalent)	Abs at 500-510 nm ; em at 530 nm → Gastric tumor cell toxicity / Reduction in mouse gastric tumor volume under illumination (PDT); generation of singlet oxygen under laser irradiation at 633 nm; → Combine fluorescence imaging / MRI / PDT	98	NA
Cobalt-ferrite NP	rhodamine B isothiocyanate (RITC)	60 (HD)	NA	Yes	NP attached to MiR124a beacon (covalent) ; RITC binds to NP in the presence of MiR124a	excitation/emission = 555/578 nm → Fluorescence when MiR124a is highly expressed / no fluorescence otherwise ; method to monitor intracellular MiR124a during neuronal differentiation	53	NA
Maghemite NP	CdSe/CdTe QD	500 (microsphre D) 7 (IONP D)	NA at RT	NA	500 Maghemite NP + 5000 CdSe/CdZnS QD embedded in a silica shell surrounding a silica microsphere	→ Manipulation of microsphere by magnetic field	76	NA
FePt NP	CdS QD	10	Ms = 5 emu/g (RT) Hc = O Oe (RT)	Yes	glutathione capping CdS QD on FePt NP (glutathione strengthens thermal stability)	Abs between 200-800 nm ; em at 420 nm for exc at 325 nm ; lifetime = 5,3 nsec (compared with 3,4 ns for free CdS QD) → FePt-CdS imaged inside RAW264.7 macrophage cells	77	NA
Fe_3O_4 NP	FITC	600-700 (D)	Ms = 17 emu/g Hc = 0 Oe	Yes	Fe_3O_4 NP mixed with polymers inside a inside a chitosan vesicle ; FITC covalently attached to chitosan	Em at 510-515 nm for exc at 475 nm Chitosan layer to avoid fluorescence quenching by iron oxide	64	NA
Fe_3O_4 NP	PyMMA FDMA	164 (D)	Hc = 0e	Yes	Fe_3O_4 + polymer and dye (Janus particle)	Fluorescence in blue and green.	187	NA
Fe_3O_4 NP	ZnS QD	100 (D)	Ms = 30 emu/g Hc = 0 Oe	NA	Fe_3O_4 NP + ZnS QD associated together in a nano sized SiO2 spheres	Abs (240-350 nm) ; em at 325 nm	78	NA
Fe_3O_4 NP	CdTe/ CdS QD	8 (D)	Hc = 0 Oe	Yes	Fe_3O_4 NP coated with dextran shell bound to QD (covalent)	Em at 600 nm for exc at 400 nm	79	NA
$Zn_{0.4}Fe_{2.6}O_4$ NP	DOX	160 (D)	Hc = 0 Oe	NA	$Zn_{0.4}Fe_{2.6}O_4$ grafted with Ad mixed with Ad-PAMAM + CD-PEI + Ad-PEG + DOX	Tumor uptake in mlice Relaease of DOX under AMF application Increase in fluorescence intensity folloing DOX release	188	NA

Table 1.3

Magnetic composition	Fluorescent substance	Size (nm)	Magnetization (MS) Coercivity (HC)	Stable (max conc.)	Type of complex containing magnetic/fluorescent substances	Fluorescent property and application	Ref	Commercialization
FePt NP	ATTO 590	5 (HD)	NA	NA	FePt NP surrounded by PMA shell containing ATTO 590	NP complex internalize preferentially inside immune cells (macrophages, dendritic cells) → increased cytokine production	59	NA
Iron oxide NP	Cy7	21 (D)	NA		IONP coated with Human Serum Albumin (HSA) + Fibroblast Growth Factor 2 + Cy7 (covalent)	Exc at 769 nm; em at 780 nm (red-shift in the absorbance spectrum between NP complex and free Cy7 dye due to dye binding to gelatin); photobleaching stabilization due to NP; → Image of cells (increase differentiation due to FGF2	57	NA
Iron oxide NP	PFVBT	180 (D)	Ms = 3 emu/g Hc = 0 Oe	NA	Iron oxide NP inserted with fluorescent polymer PFVBT inside a vesicle made of PLGA-PEG-FOL	em at 670 nm for exc at 518 nm	80	NA
Fe_3O_4 NP	fluorescent SiO_2	127 (HD)	Ms = 13 emu/g	NA	Fe_3O_4 NP surrounded by double shell (fluorescent SiO_2 + PAA); DOX incorportaed in NP complex In vitro release of DOX increased at lower pH	Abs at 480 nm; emission in green (FITC) and red (DOX) → DOX released from NP complex enters cell nucleus to perform antitumor activity	189	NA
Fe_3O_4 NP	ZnS:Mn QD	7 (D)	Ms = 10 emu/g Hc = 0^e	NA	ZnS:Mn QD sandwiched between two chitosan layers surrounding Fe_3O_4 NP	Em at 595 nm for excitation at 310 nm Chitosan prevents quanching by iron oxide (no interaction between ZnS:Mn QD and Fe_3O_4 NP	190	NA
Fe_3O_4 NP	(TOPO)-capped CdSe@ZnS QD	60	Ms = 55 emu/g Hc = 0 Oe	NA	Fe_3O_4 coated with PEI ; QD assembled on PEI (covalent) ; TAT peptide attached	Abs peak at 578 nm ; emission at 592 nm; Cell internalization of NP complex in perinuclear region	81	NA
Fe_3O_4 NP	FITC	36 (HD)	Ms = 23 emu/g Hc = 0 Oe	NA	Fe_3O_4 NP grafted with P(PEGMA) bound to FITC (covalent)	NP inside breast cancer cell imaged by fluorescence (85 pg Fe of NP per cell)	65	NA
Fe_3O_4 NP	PDI–PAA	60 (D)	Ms = 7 emu/g Hc = 0 Oe	Yes	Fe_3O_4 NP coated by SiO_2–PDI–PAA/Ca^{2+}	Em at 626 nm for exc at 540 nm Slica shell prevents fluorescence quenching → For NP incubated with Hela cells, fluorescence intensity increases with incubation time / NP concentration	191	NA
Fe_3O_4 NP	squarylium indocyanine	51 (D)	Ms = 8 emu/g Hc = 0 Oe	NA	Fe_3O_4 NP coated by SiO_2–CMCS-dye	Abs at 638 nm; em at 647 nm NP internalize in cells with nucleic acids → intracellular nucleic acid accumulation	192	NA
Maghemite NP	rhodamine derivative (RITC)	20-40	Ms = 60 emu/g Hc = 0 Oe	Yes	Maghemite NP stablized by OH- groups bound to positively charged RITC (electrostic interactions)	Immobilization of glucose oxidase on NP complex (covalent) → biosensor to remove oxygen in the presence of excess of glucose	54	NA

Table 1.4

Magnetic composition	Fluorescent substance	Size (nm)	Magnetization (MS) Coercivity (HC)	Stable (max conc.)	Type of complex containing magnetic/fluorescent substances	Fluorescent property and application	Ref	Commercialization
Magnetite NP	coumarin-153	11 (ND) 5-10 µm (NW length)	Ms = 6 emu/g	Yes	Magnetite NP + Coumarin in PS NW.	Em at 524 nm for exc at 457 nm → NW can be functionalized with antibodies. → NW bind to epithelial lung cancer cell (A549) receptor / endocytotic internalisation for short NW → Alignment of NW in direction of applied magnetic field	104	NA
Fe_3O_4 NP	$NaYF_4$: Yb, Er	100-150 (D)	Ms = 3 emu/g Hc = 0 Oe	Yes	Covalent binding between carboxyl-functionalized Fe_3O_4 NP and amino-functionalized silica-coated fluorescent $NaYF_4$: Yb,Er NP + conjugated with transferin	em at 500-575 nm under exc at 980 nm → Bindindg of NP complex at cell surface due to transferrin → Labeling and fluorescent imaging of HeLa cells + cellular magnetic separation	94	NA
$CoFe_2O_4$	DOX	120 (D)	Ms = 51 emu/g Hc = 0 Oe	Yes	$CoFe_2O_4$ surrounded by mesoporous carbon nanosphere containing DOX	Em at 450 nm under exc at 360 nm → CoFe2O4@mC@DOX exhibit more cytotoxic than free DOX towards HeLa cells → Percentage of DOX released from NP complex larger at pH 4 (70%) than pH 7 (15%)	193	NA
Magnetite NP	Cy5.5	98 (HD)	Hc = Oe	Yes	Magnetite NP surrounded by silica bound to Cy5.5 + PEG + peptide gH625 (covalent)	→ NP complex prevents fluorophore from quenching and release from NP → Enhanced cellular internalization with peptide	58	NA
Maghemite NP	PyMA	60 (D)	Hc = 0 Oe NA	NA	Glycocopolymer (MAGal) + (PyMA) attached to silica shell surrounding maghemite NP (thiol–ene chemistry)	Em at 475 nm under excitation at 317 nm → Galactose facilitates internalization in mammalian cells such as A549 cells (targeting of cell nucleus)	99	NA
Fe_3O_4 NP	FITC	88 (D)	Ms = 74 emu/g Hc ≠ 0 Oe	No	Fe_3O_4 covered with SiO_2 shell bound to FITC covalently bound to PEI	→ Used for cell (neuroblast) imaging	66	NA
Iron oxide NP	DOX + ICG	20-30 (D)	Hc = 0 Oe	Yes	Iron oxide NP stabilized with DSPE-PEG 2000 ; hydrophobic DOX and amphiphilic ICG incorporated in phospholipid layer outside iron oxide NP core by hydrophobic interaction	→ NP complex administered C6 glioma-bearing rats cross BBB, localize in tumor as reveled by fluorescence, release DOX.	16	NA
Maghemite NP	Rhodamine (Rh) congo red (CR)	15 (D)	Hc = 0 Oe	NA	Electrostatic interaction of CR with IONP surface; Covalent attachment between RhB and IONP	→ NP complex selectively marks Ab40 fibrils; → early detection of plaques by fluorescence/MRI; → Diagnosis of Alzheimer disease	51	NA
Fe_3O_4 NP	CdSe QD	600 (D)	Hc = 0 Oe	Yes	CdSe QD + Fe_3O_4 NP in hollow silica sphere	Em at 617 nm for exc at 232 nm Cell labeling by fluorescence; enhancement of fluorescence for NP complex conjugated witrh folic acid	89	NA
Fe_3O_4 NP	FITC DOX	160 (D)	Hc = 0 Oe	NA	Fe_3O_4 NP surrounded by silica / FITC / P(HEMA) / P(NIPAAM-co-AA) ; DOX loaded in thermo/pH sensitive NP	→ NP used for DOX release increased at low pH; → Cytotoxicity towards HeLa cells	67	NA

Table 1.5

Magnetic composition	Fluorescent substance	Size (nm)	Magnetization (MS) Coercivity (HC)	Stable (max conc.)	Type of complex containing magnetic/fluorescent substances	Fluorescent property and application	Ref	Commercialization
Fe_3O_4 NP	ZnSe NP	6.8 (Fe_3O_4 NP D) 3.5 (ZnSe NP D)	Hc = 0 Oe (RT)	NA	Fe_3O_4 NP seed for growth of ZnSe NP Fe_3O_4 NP core surrounded by shell of ZnSe NP .	Exc at 325 nm; em at 390 nm for Fe_3O_4/ZnSe NP (compared with exc at 377 nm and em at 433 nm for free ZnSe NP); QY ↓ from 10% for free ZnSe NP to 1% for Fe_3O_4/ZnSe NP; → Effects due to: i) change in shape between spherical ZnSe NP and ZnSe emitters in core/shell NP, ii) carrier leakage at interface between Fe_3O_4 and ZnSe NP in core/shell structure	82	NA
Fe_3O_4 NP	RITC + FITC	NA	Hc = 0 Oe	NA	Fe_3O_4 NP stabilized with PEG/dextran/FITC/RITC bound to antibodies (covalent).	Antibodies associated with Fe_3O_4 NP bind to SIRPA or KDR membrane receptors on cardiac progenitor cells → labeling of cardiac progenitor cells.	55	NA
Fe_3O_4 NP	FITC	86 (D)	Hc = 0 Oe Ms = 73 emu/g	NA	Fe_3O_4 NP and FITC incorporated in silica bound to chlorotoxin (covalent)	→ NP complex photostable → specifically internalizes in U251-MG glioma cells (endocytosis)	68	NA
Fe_2O_3 Beads	CdSe/ZnS QD	30 (D)	Hc = 0 Oe	NA	Fe_2O_3 NP Core surrounded by a shell of CdSe/ZnS QD; anticycline E antibodies attached to surface of NP complex (covalent)	→ NP complex fluoresce in green and red. → NP complex ↓ in QY + blue shift to lower wavelength of emission peak compared with free CdSe/ZnS QD. → Anticycline E antibodies bind specifically to cycline protein expressed on breast cancer cell surface. → Separation of breast cells observed by fluorescence imaging microscopy.	83	NA
Magnetite NP	FITC	100 (HD)	Hc = 0 Oe Ms = 20 emu/g (Ms = 60 emu/g for Fe_3O_4 NP)	NA	Fe_3O_4 NP coated by PLMA bound to FITC (covalent).	→ NP complex not cytotoxic towards 3T3 fibroblasts and human mesenchymal stem cells (hMSCs); → Detection of hMSCs labeled with NP complex by MRI (T2) and Fluorescence (green).	32	NA
Magnetite NP	YPO_4:Re (Re = Tb, Eu)	500-600 (D)	Hc = 0 Oe (RT)	NA	YPO_4 :Re spheres containing Fe_3O_4 NP + DOX bound to spheres.	Exc at 224 nm; em 530-560 nm (Tb) and 580-650 nm (Eu); → Release of DOX in vitro from DOX-Fe_3O_4@YPO_4 → Internalization of DOX-Fe_3O_4@YPO_4 : Tb in Hela cells observed by fluorescence	194	NA
$CoFe_2O_4$	PFV	35 (D)	Hc = 0 Oe	Yes	$CoFe_2O_4$ covered by silica shell; PDDA/PSS layers assembled on silica; PFV adsorbed on PSS; heparin bound to PFV to increase cellular uptake / biocompatibility of NP complex	→ NP complex used to image cells by fluorescence	195	NA
Fe_3O_4 NP	CdTe	50 (D)	NA	Yes	Fe_3O_4 NP + CdTe in Silica bound to BRCAA1 monoclonal antibody (covalent)	→ Gastric cancer cells overexpress BRCAA1 proteins; → NP complex display very low toxicity; → NP complex endocytosed by gastric cancer MGC803 cells,; → NP complex targets in vivo mouse gastric cancer tumor tissues (imaged by fluorescent and MRI).	84	NA
Fe_3O_4 NP	FITC	50 (D)	Hc = 0 Oe Ms = 2 emu/g	Yes (no photobl eaching)	Fe_3O_4 NP surrounded by a first shell of silica containing FITC and a second shell of mesoporous silica ; AlC_4Pc in mesoporous silica ; FA attached at the surface of mesoporous silica.. FITC; Al_4Pc, FA covalently attached	Exc at 488 nm → em at 520 nm (FITC). Exc at 620 nm → em at 695 nm (AlC4Pc) → NP complex suitable for fluorescence imaging / PDT → NP complex kill 50% of hepatoma cancer cells by PDT (660 nm laser at 75 mW cm^2, 800 µg/mL of NP)	196	NA
Fe_3O_4 NP	DNA_{GFP} DNA_{DsRed}	220 (HD)	Hc = 0 Oe	Yes	Fe_3O_4 NP surrounded by a shell of PEI attached to DNA_{GFP} / DNA_{DsRed} (few 100 nm of DNA strands bound to Fe_3O_4 NP)	→ Expression of GFP / DsRed in porcine kidney PK-15 cells by magnetofection.	197	NA

Table 1.6

Magnetic composition	Fluorescent substance	Size (nm)	Magnetization (MS) Coercivity (HC)	Stable (max conc.)	Type of magnetic/fluorescent nanocomplex	Fluorescent property and application	Ref	Commercialization
Magnetite	FITC	115 nm (HD)	Hc = 0 Oe Ms = 27 emu/g	Yes	PEG-FITC polymer matrix encapsulates magnetite NP + DOX ;	Cellular toxicity of NP towards HeLa cells; possibility to release DOX; Tumor growth delay in HeLa tumor-bearing mice after intravenous injection of NP complex	198	NA
Fe_3O_4 NP	fluorescent carbon (FC)	9 (Fe_3O_4 D) 3 (FC D)	Hc = 0 Oe Ms = 13 emu/g	Yes	Fe_3O_4 NP core covered by a fluorescent carbon shell	→ NP can be imaged by fluorescence → NP exposed to 825 nm ; 1.5 W cm^{-2} for 5 min destroy HEK293T cells through heat generation (PTT); → Tumor growth retardition in mice bearing C6 glioblastoma treated by PTT	101	NA
Fe_3O_4 NP	Cy5	NA	Hc = 0 Oe	Yes	Fe_3O_4 NP, PAMAM-G4-NH2 dendrimer, Cy5, attached on graphene oxide (covalent)	→ NP complex internalize in MCF-7 breast cancer cells (fluorescence of cells) → NP complex non-toxic to MDA-MB-231 cell growth, (in contrast to free G4 dendrimer and GO-G4 conjugate)	105	NA
F_3O_4 NP	CdSe/ZnS QD	395 (Microbead HD)	Ms = 25 emu/g	Yes	Fe_3O_4 + QD inside silica microbead	→ Isolation of target tumor cells; → cancer diagnosis (medical imaging); → cancer therapy (targeted drug delivery);	85	NA
Fe_3O_4 NP	Ruthenium (Ru) complex	43 (HD)	Hc = 0 Oe Ms = 40 emu/g	Yes	Fe_3O_4 coated with PPG-PEGPPG-diamine bound to Ru; Fe_3O_4 coated with DHPPA bound to Ru;	Em at 740 nm for exc at 490 nm → NP complex does not release a detectable amount of Ru; → NP complex incubated with SK-BR-3 cells (cell imaging by fluorescence)	199	NA
Fe_3O_4 NP	Eu complex	8 (Fe_3O_4 NP D)	Hc = 0 Oe Ms = 43 emu/g	Yes	Fe_3O_4–DPA–PEG–BMAP–Eu NP conjugate: Fe3O4 NP modified with DPA and PEG diacid, conjugated with Eu(III) complex of BMAP.	Exc at 395 nm; em at 615 nm; → No cytotoxicity towards SK-BR-3 cells up to 100 µg/mL NP; → Imaging of SK-BR-3 cells by fluorescence imaging;	200	NA
Iron oxide NP (IONP)	Up Conversion NP (UPCNP)	150-200 (D)	Hc = 0 Oe Ms = 50 emu/g	Yes	NP complex containing: Dye/drug, UPCNP, IONP, polymer mixed together	→ Combination of upconversion luminescence (UCL) with down-conversion fluorescence (FL) (dye is Squaraine)	201	NA
F_3O_4 NP	carbazole	146 (HD)	Hc = 0 Oe Ms = 9 emu/g (Ms = 18 emu/g for Fe_3O_4 NP)	Yes	PEGylated micelles containing Fe_3O_4 ; carbazole in polymer shell of micelle	→ Em at 350-360 nm for exc at 294 nm → No cytotoxicity towards HeLa cells (up to 1 mg/mL of NP complex); → Blue fluorescence of liver/spleen cells incubated with NP complex	103	NA
$CoFe_2O_4$ NP	PDI-4NH_2	106 (HD)	NA	NA	$CoFe_2O_4$ NP coated by dopamine + HSA + PDI-4NH_2 (non-covalent)	Exc at 500 nm, em at 548 nm; NP complex biocompatibility; NP complex internalizes in cells (free PDI-4NH_2 does not internalize);	202	NA
Fe_3O_4 NP	Mn:ZnS QD	93 (D)	Hc = 0 Oe		PLGA vesicles containing Fe_3O_4 NP + Mn:ZnS QD + busulfan (anti-cancer drug)	→ NP complex internalizes in Murine macrophage (J774A) cells (imaged by MRI + fluorescence); → Drug/busulfan delivery ability of NP complex demonstrated in vitro.	86	NA

Table 1.7

Magnetic composition	Fluorescent substance	Size (nm)	Magnetization (MS) Coercivity (HC)	Stable (max conc.)	Type of magnetic/fluorescent nanocomplex	Fluorescent property and application	Ref	Commercialization
Fe_3O_4 NP	IR-820 dye	6	NA	Yes	Amphiphilic polymer (poly-isobutylene-alt-maleic anhyride)) functionalized with IR-820 dye surrounding Fe_3O_4 NP	→ NP complex has wide emission range (800 to 1000 nm); → NP complex displays minimal cytotoxicity; → NP complex used for labeling of cancerous HeLa cells (NIR fluorescence microscopy); → NP complex displays good negative contrast enhancement in T2-weighted MR imaging in murine model.	203	NA
Fe_3O_4 NP	CdTe QD	70-90 (NP complex D) 14 (Fe_3O_4 NP)	Hc = 0 Oe Ms = 5 emu/g	Yes	Fe_3O_4 NP covered by mesoporous silica shell ; layer-by-layer assembly of 3-aminopropyltrimethoxysilane and fluorescent CdTe QD on SiO_2 surface.	→ PL Emission at 660 nm → Mesoporous silica has large loading capacity (application for drug delivery/targeting).	87	NA
Fe_3O_4 NP	FITC ; RITC	28 (NP complex D) 9 nm (Fe_3O_4 NP)	Hc = 0 Oe Ms (2 emu/g for NP complex) Ms = 30 emu/g for Fe_3O_4 NP	Yes	Fe_3O_4 NP covered by amorphous silica shell containing dye (FITC/RITC) inside	→ Em at 522 nm for exc at 470 nm (NP complex with FITC) → Em at 572 nm for exc at 520 cm (NP complex with RITC) → NP complex used for HeLa cell imaging;	118	NA
Fe_3O_4 NP	RITC	63 (NP complex D)	Hc = 0 Oe Ms = 19 emu/g	Yes	Fe_3O_4 NP coated by PEI surrounded by fluorescent mesoporous silica ; siRNA in electrostatic interaction with PEI	→ Em at 550 nm; → Delivery of siRNA (magnetically guided and followed by fluorescence);	172	NA
Fe_3O_4 NP	Cy5.5	138 (NP complex HD)	Hc = 0 Oe	Yes	NP complex made of Fe_3O_4 NP coated by PEI first layer attached to Cy5.5 (covalent) ; second layer of PEG bound to PEI first layer (covalent); HCBP-1 peptide bound to PEG (covalent);	→ Ex = 675 nm, Em = 695 nm; → NP complex good hemo-compatibility and low cytotoxicity; → NP complex can isolate HCBP-1 positive cancer cells in vitro; → NP complex can be used for cancer stem cell detection;	106	NA
Fe_3O_4 NP	Eu^{3+}	76 (NP complex) 13 (Fe_3O_4 NP)	Hc = 0 Oe		Fe_3O_4 NP covered by poly(St-NIPAM) + $Eu(AA)_3Phen$; PNIPAM: thermosensitive polymer.	→ emission peaks of Eu3+ at 594 and 619 nm; → NP complex shrinks in size with increasing temperature;	204	NA
Iron oxide NP	Fluorescent red; Cy5; Cy3; FITC; AF568; Cy5.5; Cy7.5; RhB; Indocyanine Green Dye; Fluorescent Far Red; DY-730 dye	5-300	Hc = 0 Oe	Yes	Iron oxide NP coated by cross linked dextran / hydroxyethyl starch attached to dyes	→ Cy-5 (exc 649 nm, em: 670 nm); RhB (exc 552 nm; em at 580 nm); IGD (exc at 785 nm; em at 810 nm); DY-730 dye (exc at 732 nm; em at 758 nm); Fluorescent far red (exc at 732 nm; em at 758 nm); Fluorescent red (exc at 552 nm; em at 580 nm); FITC (exc at 494 nm, em at 525 nm); Cy3 (exc at 555 nm; em at 565 nm); AF568 (exc at 578 nm; em at 605 nm); Cy5.5 (exc at 673 nm, em at 705 nm); Cy7.5 (exc at 750 nm; em at 765 nm) → Applications: Purification of targeted protein / magneto-immuno assays	Absolute Mag	CD
Cluster of several Iron oxide NP	Lipophilic fuorescent dyes (perylen derivatives)	100-200	Hc = 0 0e	Yes	Dyes are sandwiched between a magnetic core and a polysaccharide matrix	→ Blue: exc at 378 nm/ em at 413 nm; → Green: exc at 476 nm/ em at 490 nm; → Orange: exc at 524 nm / em at 539 nm; → Pink: exc at 547 nm / em at 581 nm; → Applications: Magnetic separation, labeling and fluorescence detection	nano-screen MAG (affinity)	chemicell
Iron oxide NP + organic coating	AF568, Cy3, Cy5.5, Cy5, Cy7, FITC,	5-30	Hc = 0 0e	Yes	Dyes are chemically bound to the NP	→ Applications: measure individual virus and/or exosomes by flow cytometry; Furthermore, magnetic separation/concentration of cells/proteins .	Magdye	Oceannanotech
Iron oxide NP + dextran	NA	50-100	Hc = 0 Oe	Yes	Dyes are covalently attached to NP	→ Red: exc at 552 nm / em at 580 nm; → Far-red: exc at 732 nm / em at 758 nm; → Application in hyperthermia	nanomag®-CLD-redF + synomag®-CLD-far redF	Micromod
Iron oxide NP surrounded by polymer	Cy3, Cy5, Cy5.5, RhB, fluorescein,	20-400	Hc = 0 Oe	Yes	Covalent binding between dyes and NP	→ Applications: fluorescent imaging, cellular and biomolecular labeling and magnetic sensing	MP25/350-FC/RB/Cy3/Cy5/Cy5.5	NANOCS
Iron oxide core surrounded by polystereine / silica coating comprising a dye.	NA	100-900	Hc = 0 Oe	Yes	→ Polystyrene particle core stained with solution of fluorophore; → Polymerization of fluorophore in styrene in the presence of polystyrene core particles;	→ Yellow: exc at (475 nm / em at 480 nm → Pink: exc at 560 nm / em at 580 → Nile red: exc at 510 nm / em at 555 nm → Applications: cell separation, affinity purification, DNA probe assays, magnetic particle EIA	SPHERO™ Carboxyl Fluorescent Magnetic Particles	SPHEROTECH
Magneto-somes	DiI, RhB	30-50	Hc = 250 Oe (RT)	Yes	Weak binding between iron oxide NP and dyes	→ Em at 585 nm for exc at 405 nm (RhB) → Em at 576 nm for exc at 555 nm (DiI) → Application: detection of the release of a substance of interest (drug) by fluorescence enhancement through de-quenching mechanism.	Fluorescent magnetosomes	NANOBACTERIE

Table 1.8

659

DECLARATION OF INTEREST: Edouard Alphandéry has been working in the company Nanobacterie.

ACKNOWLEDGMENT: We would like to thank the BPI (*''banque publique d'investissement, France''*), the region of Paris (*''Paris Région Entreprise, France''*), the French Research Tax Credit program (*''crédit d'impôt recherche''*), the incubator Paris Biotech Santé, the ANRT (CIFRE 2014/0359, CIFRE 2016/0747, CIFRE 2013/0364, CIFRE 2015/976), the Eurostars programs (Nanoneck-2 E9309 and Nanoglioma E11778), the AIR program (*''aide à l'innovation responsable''*) from the region of Paris (A1401025Q), the ANR (*''Agence Nationale de la Recherche''*) Méfisto, as well as the Universities Paris 6 and Paris 11. We also would like to thank the Nomis Foundation and Markus Reinhard for their support.

REFERENCES:

1. Yang Y, Wang L, Wan B, Gu Y, Li X, Optically Active Nanomaterials for Bioimaging and Targeted Therapy, Front. Bioeng. Biotechnol., 2019; 7: 320.

2. Zhang Y, Li M, Gao X, Chen Y, and Liu T, Nanotechnology in cancer diagnosis: progress, challenges and opportunities. Journal of Hematology & Oncology 2019; 12: 137.

3. Padmanabhan P, Kumar A, Kumar S, Chaudhary RK, Gulyás B, Nanoparticles in practice for molecular-imaging applications: An overview. Acta Biomaterialia 2016; 41: 1–16

4. Alphandéry E, Iron oxide nanoparticles as multimodal imaging tools. RSC Adv., 2019; 9: 40577-40587.

5. Shen Z, Wu A, Chen X, Iron Oxide Nanoparticle Based Contrast Agents for Magnetic Resonance Imaging, Mol. Pharmaceutics 2017; 14: 1352−1364.

6. Bouziotis P, Psimadas D, Tsotakos T, Stamopoulos D, Tsoukalas C, Radiolabeled Iron Oxide Nanoparticles As Dual-Modality SPECT/MRI and PET/MRI Agents, Current Topics in Medicinal Chemistry 2012; 12: 2694-2702

7. Song K, Lee S, Suh CY, Kim W, Ko KS, Shin D, Synthesis and Characterization of Iron Oxide Nanoparticles Prepared by Electrical Explosion of Fe Wire in ArO2 Gas Mixtures, Materials Transactions 2012; 53: 2056-2059.

8. Kim W, Suh CY, Cho SW, Roh KM, Kwon H, Song K, Shon IJ, A new method for the identification and quantification of magnetite–maghemite mixture using conventional X-ray diffraction technique, Talanta 2012; 94: 348– 352.

9. Rosenfeldt S, Riese CN, Mickoleit F, Schüler D, Schenk AS, Probing the Nanostructure and Arrangement of Bacterial Magnetosomes by Small-Angle X-Ray Scattering, Appl Environ Microbiol 2019; 85: e01513-19

10. Alphandéry E, Biodistribution and targeting properties of iron oxide nanoparticles for treatments of cancer and iron anemia disease, Nanotoxicology 2019; 13: 573–596.

11. Maier-Hauff K, Ulrich F, Nestler D, Niehoff H, Wust P, Thiesen B, Orawa H, Budach V, Jordan A, Efficacy and safety of intratumoral thermotherapy using magnetic iron-oxide nanoparticles combined with external beam radiotherapy on patients with recurrent glioblastoma multiforme, J Neurooncol 2011; 103: 317–324.

12. Maier-Hauff K, Rothe R, Scholz R, Gneveckow U, Wust P, Thiesen B, Feussner A, von Deimling A, Waldoefner N, Felix R, Jordan A, Intracranial thermotherapy using magnetic nanoparticles combined with external beam radiotherapy: Results of a feasibility study on patients with glioblastoma multiforme, J Neurooncol 2007; 81: 53–60.

13. Estelrich J, Busquets MA, Iron Oxide Nanoparticles in Photothermal Therapy, Molecules 2018; 23: 1567.

14. Israel LL, Galstyan A, Holler E, Ljubimova JY, Magnetic iron oxide nanoparticles for imaging, targeting and treatment of primary and metastatic tumors of the brain, Journal of Controlled Release 2020; 320: 45–62.

15. Jayapaul J, Hodenius M, Arns S, Lederle W, Lammers T, Comba P, Kiessling F, Gaetjens J, FMN-coated fluorescent iron oxide nanoparticles for RCP-mediated targeting and labeling of metabolically active cancer and endothelial cells, Biomaterials 2011; 32: 5863-5871.

16. Shen C, Wang X, Zheng Z, Gao C, Chen X, Zhao S, Dai Z, Doxorubicin and indocyanine green loaded superparamagnetic iron oxide nanoparticles with PEGylated phospholipid coating for magnetic

resonance with fluorescence imaging and chemotherapy of glioma, International Journal of Nanomedicine 2019; 14: 101–117.

17. Alphandéry E, Natural Metallic Nanoparticles for Application in Nano-Oncology, Int. J. Mol. Sci. 2020; 21: 4412.

18. Zhao S, Yu X, Qian Y, Chen W, Shen J, Multifunctional magnetic iron oxide nanoparticles: an advanced platform for cancer theranostics, Theranostics 2020; 10: 6278-6309.

19. Lacroix LM, Delpech F, Nayral C, Lachaize S, Chaudret C, New generation of magnetic and luminescent nanoparticles for in vivo real-time imaging, Interface Focus 2013; 3: 20120103.

20. Lartigue L, Coupeau M, Lesault M, Luminophore and Magnetic Multicore Nanoassemblies for Dual-Mode MRI and Fluorescence Imaging, Nanomaterials 2020; 10: 28.

21. García RS, Stafford S, Gun'ko Y, Recent Progress in Synthesis and Functionalization of Multimodal Fluorescent-Magnetic Nanoparticles for Biological Applications. Appl. Sci. 2018; 8: 172.

22. Alphandéry E, Haidar DA, Seksek O, Thoreau M, Trautmann, A, Bercovici N, Gazeau F, Guyot F, Chebbi I, Nanoprobe Synthesized by Magnetotactic Bacteria, Detecting Fluorescence Variations under Dissociation of Rhodamine B from Magnetosomes following Temperature, pH Changes, or the Application of Radiation, ACS Appl. Mater. Interfaces 2017; 9: 36561-36572.

23. Alphandéry E, Haidar DA, Seksek O, Guyot F, Chebbi I, Fluorescent magnetosomes for controlled and repetitive drug release under the application of an alternating magnetic field under conditions of limited temperature increase (<2.5 °C), Nanoscale, 2018; 10: 10918-10933.

24. Shcherbakova, DM, Baloban, M, Verkhusha, VV, Near-infrared fluorescent proteins engineered from bacterial phytochromes, Curr Opin Chem Biol., 2015; 27: 52–63.

735 25. Fischer, A, Schmitz, M, Aichmayer, B, Fratzl, P, Faivre, D, Structural purity of magnetite
736 nanoparticles in magnetotactic bacteria, J. R. Soc. Interface, 2011; 8: 1011–1018.

737 26. Mahadevan, S, Behera, SP, Gnanaprakash, G,,Jayakumar, T, Philip J, Rao, BPC, Size distribution
738 of magnetic iron oxide nanoparticles using Warren–Averbach XRD analysis, Journal of Physics and
739 Chemistry of Solids, 2012; 73: 867–872

740 27. Sun YK, Ma M, Zhang Y, Gu N, Synthesis of nanometer-size maghemite particles from magnetite,
741 Colloids and Surfaces A: Physicochem. Eng. Aspects 2004; 245: 15–19

742 28. Szczerba W, Costo R, Veintemillas-Verdaguer S, Del Puerto Morales M, Thunemann A F, SAXS
743 analysis of single- and multi-core iron oxide magnetic nanoparticles, J. Appl. Cryst. 2017; 50: 481–488.

744 29. Lim J, Yeap SP, Che HX, Low SC, Characterization of magnetic nanoparticle by dynamic light
745 scattering, Nanoscale Research Letters 2013; 8: 381.

746 30. Yang SC, Paik SYR, Ryu J, Choi KO, Kang TS, Lee JK, Song CW, Ko S, Dynamic light
747 scattering-based method to determine primary particle size of iron oxide nanoparticles in simulated
748 gastrointestinal fluid, Food Chemistry 2014; 161: 185–191

749 31. Carvalho PM, Felício MR, Santos NC, Gonçalves S, Domingues MM, Application of Light
750 Scattering Techniques to Nanoparticle Characterization and Development, Frontiers in Chemistry 2018;
751 6: 237.

752 32. Wang L, Neoh KG, Kang ET, Shuter B, Wang SC, Biodegradable magnetic fluorescent
753 magnetite/poly(DL-lactic acid-co-a,b-malic acid) composite nanoparticles for stem cell labeling,
754 Biomaterials 2010; 31: 3502–3511.

33. Rao YF, Chen W, Liang XG, Huang YZ, Miao J, Liu L, Lou Y, Zhang XG, Wang B, Tang RK, Chen Z, Lu XY, Epirubicin-Loaded Superparamagnetic Iron-Oxide Nanoparticles for Transdermal Delivery: Cancer Therapy by Circumventing the Skin Barrier, Small 2015; 11: 239–247.

34. Azadmanjiri J, Simon GP, Suzuki K, Selomulya C, Cashion JD, Phase reduction of coated maghemite (g-Fe2O3) nanoparticles under microwave-induced plasma heating for rapid heat treatment, J. Mater. Chem. 2012; 22: 617-625.

35. Lesiak B, Rangam N, Jiricek P, Gordeev I, Tóth J, Kövér L, Mohai M, Borowicz P, Surface Study of Fe3O4 Nanoparticles Functionalized With Biocompatible Adsorbed Molecules, Frontiers in Chemistry, 2019; 7: 642.

36. Shi D, Sadat ME Dunn AW, Mast DB, Photo-fluorescent and magnetic properties of iron oxide nanoparticles for biomedical applications, Nanoscale, 2015; 7: 8209-8232.

37. Loudet A., Burgess K, BODIPY dyes and their derivatives: syntheses and spectroscopic properties, Chem. Rev. 2007; 107: 4891−4932.

38. Yu CJ, Wu SM, Tseng WL, Magnetite Nanoparticle-Induced Fluorescence Quenching of Adenosine Triphosphate−BODIPY Conjugates: Application to Adenosine Triphosphate and Pyrophosphate Sensing, Anal. Chem. 2013; 85: 8559−8565.

39. Amendola V, Saija R, Maragò OM, Iatì MA, Superior plasmon absorption in iron-doped gold nanoparticles, Nanoscale, 2015; 7: 8782-8792.

40. Reguera J, de Aberasturi DJ, Henriksen-Lacey M, Langer J, Espinosa A, Szczupak B, Wilhelmd C, Liz-Marzán LM. Janus plasmonic–magnetic gold–iron oxide nanoparticles as contrast agents for multimodal imaging, Nanoscale, 2017, 9, 9467-9480

41. Levin CS, Hofmann C, Ali TA, Kelly AT, Morosan E, Nordlander P, Whitmire KH, Halas NJ, Magnetic-Plasmonic Core-Shell Nanoparticles, ACS Nano, 2009; 3: 1379–1388.

42. Ramade J, Cottancin E, Lebeault MA, Langlois C, Piccolo L, Broyer M, Environmental Plasmonic Spectroscopy of Silver−Iron Nanoparticles: Chemical Ordering under Oxidizing and Reducing Conditions, J. Phys. Chem. C 2019; 123: 15693−15706.

43. Noguez C, Surface Plasmons on Metal Nanoparticles: The Influence of Shape and Physical Environment, J. Phys. Chem. C 2007; 111: 3806-3819.

44. Alphandéry E, Ngo AT, Lefèvre C, Lisiecki,I, Wu LF, Pileni MP, Difference between the Magnetic Properties of the Magnetotactic Bacteria and Those of the Extracted Magnetosomes: Influence of the Distance between the Chains of Magnetosomes, J. Phys. Chem. C 2008; 112: 12304–12309.

45. Testa-Anta M, Ramos-Docampo MA, Comesana-Hermo M, Rivas-Murias B, Salgueirino V, Raman spectroscopy to unravel the magnetic properties of iron oxide nanocrystals for biorelated applications, Nanoscale Adv., 2019, 1, 2086-2103.

46. Dutz S, Buske N, Landers J , Gräfe C, Wende H, Clement JH, Biocompatible Magnetic Fluids of Co-Doped Iron Oxide Nanoparticles with Tunable Magnetic Properties, Nanomaterials, 2020; 10: 1019.

47. Leyssens L, Vinck B, Van Der Straeten C, Wuytse F, Maes L, Cobalt toxicity in humans—A review of the potential sources and systemic health effects, Toxicology 2017; 387: 43–56.

48. Byrne JM, Coker VS, Cespedes E, Wincott PL, Vaughan DJ,Pattrick RAD, Biosynthesis of Zinc Substituted Magnetite Nanoparticles with Enhanced Magnetic Properties, Adv. Funct. Mater. 2014; 24: 2518–2529.

49. Bertorelle F, Wilhelm C, Roger J, Gazeau F, Ménager C, Cabuil V, Fluorescence-Modified Superparamagnetic Nanoparticles: Intracellular Uptake and Use in Cellular Imaging, Langmuir 2006; 22: 5385-5391.

50. Gallagher JJ, Tekoriute R, O'Reilly J-A, Kerskens C, Gun'ko YK, Lyncha M, Bimodal magnetic-fluorescent nanostructures for biomedical applications, J. Mater. Chem., 2009; 19: 4081–4084.

51. Skaat H, Margel S, Synthesis of fluorescent-maghemite nanoparticles as multimodal imaging agents for amyloid-b fibrils detection and removal by a magnetic field, Biochemical and Biophysical Research Communications, 2009; 386: 645–649.

52. Cho YS, Yoon TJ, Jang ES, Hong KS, Lee SY, Kim OR, Park C, Kim YJ, Yi GC, Chang K, Cetuximab-conjugated magneto-fluorescent silica nanoparticles for in vivo colon cancer targeting and imaging, Cancer Letters, 2010; 299: 63–71.

53. Hwang DW, Song IC, Lee DS, Kim S, Smart Magnetic Fluorescent Nanoparticle Imaging Probes to Monitor MicroRNAs, Small, 2010; 6: 81–88.

54. Magro, M, Sinigaglia G, Nodari, L, Tucek, J, Polakova, K, Marusak Z, Charge binding of rhodamine derivative to OH stabilized nanomaghemite: Universal nanocarrier for construction of magnetofluorescent biosensors, Acta Biomaterialia, 2012; 8: 2068–2076.

55. Verma VK, Kamaraju SR, Kancherla R, Kona LK, Beevi SS, Debnath T, Usha SP, Vadapalli R, Arbab AS, Chelluri LK, Fluorescent magnetic iron oxide nanoparticles for cardiac precursor cell selection from stromal vascular fraction and optimization for magnetic resonance imaging, International Journal of Nanomedicine, 2015; 10: 711–726.

56. Fu A, Wilson RJ, Smith BR, Mullenix J, Earhart C, Akin D, Guccione S, Wang SX, Gambhir SS, Fluorescent Magnetic Nanoparticles for Magnetically Enhanced Cancer Imaging and Targeting in Living Subjects, ACSnano, 2012; 6: 6862–6869

57. Levy I, Sher I, Corem-Salkmon E, Ziv-Polat1 O, Meir A, Treves AJ, Nagler A, Kalter-Leibovici O, Margel S, Rotenstreich Y, Bioactive magnetic near Infra-Red fluorescent core-shell iron oxide/human serum albumin nanoparticles for controlled release of growth factors for augmentation of human mesenchymal stem cell growth and differentiation. Journal of Nanobiotechnology, 2015; 13: 34.

58. Perillo E, Hervé-Aubert K, Allard-Vannier E, Falanga A, Galdiero S, Chourpa I, Synthesis and in vitro evaluation of fluorescent and magnetic nanoparticles functionalized with a cell penetrating peptide for cancer theranosis,. Journal of Colloid and Interface Science, 2017; 499: 209–217.

59. Lehmann AD, Parak WJ, Zhang F, Ali Z, Rocker C, Nienhaus GU, Fluorescent–Magnetic Hybrid Nanoparticles Induce a Dose-Dependent Increase in Proinflammatory Response in Lung Cells in vitro Correlated with Intracellular Localization, Small, 2010; 6: 753–762.

60. Howes P, Green M, Bowers A, Parker, D, Varma, G, Kallumadil M, Magnetic Conjugated Polymer Nanoparticles as Bimodal Imaging Agents, J. Am. Chem. Soc. 2010, 132: 9833–9842.

61. Chekina N, Horak D, Jendelova P, Trchova M, Benes M J, Hruby M, Herynek V, Turnovcov K, Sykova E, Fluorescent magnetic nanoparticles for biomedical applications, J. Mater. Chem., 2011; 21: 7630-7639.

62. Ebrahiminezhad A, Ghasemi Y, Rasoul-Amini S, Barar J, Davarana S, Preparation of novel magnetic fluorescent nanoparticles using amino acids, Colloids and Surfaces B: Biointerfaces, 2013; 102: 534– 539.

63. Ge Y, Zhang Y, He S, Nie F, Teng G, Gu N, Fluorescence Modified Chitosan-Coated Magnetic Nanoparticles for High-Efficient Cellular Imaging, Nanoscale Res Lett, 2009; 4: 287–295.

64. Kaewsaneha C, Opaprakasit P, Polpanich D, Smanmoo S, Tangboriboonrat P, Immobilization of fluorescein isothiocyanate on magnetic polymeric nanoparticle using chitosan as spacer Journal of Colloid and Interface Science, 2012; 377: 145–152.

65. Lu X, Jiang R, Fan O, Zhang L, Zhang H, Yang M, Fluorescent-magnetic poly(poly(ethyleneglycol)monomethacrylate)-grafted Fe3O4 nanoparticles from post-atom-transfer-radical-polymerization modification: synthesis, characterization, cellular uptake and imaging, J. Mater. Chem., 2012; 22: 6965-6973.

66. Pinheiro PC, Daniel-da-Silva AL, Tavares DS, Calatayud MP, Goya GF, Trindade T, Fluorescent Magnetic Bioprobes by Surface Modification of Magnetite Nanoparticles, Materials 2013; 6: 3213-3225.

67. Torkpur-Biglarianzadeh M, Salami-Kalajahi M, Multilayer fluorescent magnetic nanoparticles with dual thermoresponsive and pH-sensitive polymeric nanolayers as anti-cancer drug carriers, RSC Adv., 2015, 5, 29653-29662.

68. Wan J, Meng X, Liu E, Chen K, Incorporation of magnetite nanoparticle clusters in fluorescent silica nanoparticles for high-performance brain tumor delineation, Nanotechnology, 2010; 21: 235104.

69. Alander JT, Kaartinen I, Laakso A, Patila T, Spillmann T, Tuchin VV, A Review of Indocyanine Green Fluorescent Imaging in Surgery, International Journal of Biomedical Imaging, 2012; Article ID 940585.

70. Chen O, Riedemann L, Etoc F, Herrmann H, Coppey M, Barch M, Farrar CT, Zhao J, Bruns OT, Wei H, Guo P, Cui J, Jensen R, Chen Y, Harris DK, Cordero JM, Wang Z, Jasanoff A, Fukumura D, Reimer R, Dahan M, Jain RK, Bawendi MG, Magneto-Fluorescent Core-Shell Supernanoparticles, Nat Commun, 2014; 5: 5093.

71. Cho HS, Dong Z, Pauletti GM, Zhang,J, Xu H, Gu H, Wang L, Ewing RC, Huth C, Wang F,† Shi D, Fluorescent, Superparamagnetic Nanospheres for Drug Storage, Targeting, and Imaging:AMultifunctional Nanocarrier System for Cancer Diagnosis and Treatment, ACSNano, 2010; 4, 5398-5404.

72. Cho M, Contreras EQ, Lee, SS, Jones, CJ, Jang, W, Colvin VL, Characterization and Optimization of the Fluorescence of Nanoscale Iron Oxide/Quantum Dot Complexes, J. Phys. Chem. C 2014; 118, 14606−14616.

73. Ding Y, Yin H, Shen S, Sun K, Liu F, Chitosan-based magnetic/fluorescent nanocomposites for cell labelling and controlled drug release, NewJ.Chem., 2017; 41: 1736-1743.

74. Gui R, Wang Y, Sun J, Encapsulating magnetic and fluorescent mesoporous silica into thermosensitive chitosan microspheres for cell imaging and controlled drug release in vitro, Colloids and Surfaces B: Biointerfaces, 2014; 113: 1– 9.

75. Hong X, Li J, Wang M, Xu J, Guo W, Li J, Bai Y, Li T, Fabrication of Magnetic Luminescent Nanocomposites by a Layer-by-Layer Self-assembly Approach, Chem. Mater. 2004; 16: 4022-4027.

76. Insin N, Tracy, JB, Lee H, Zimmer JP, Westervelt RM, Bawendi MG, Incorporation of Iron Oxide Nanoparticles and Quantum Dots into Silica Microspheres. ACSNano, 2008; 2: 197-202.

77. Jha DK, Saikia K, Chakrabarti S, Bhattacharya K, Varadarajan KS, Patel AB, Goyary D, Deba C, Direct one-pot synthesis of glutathione capped hydrophilic FePt-CdS nanoprobe for efficient bimodal imaging application. Materials Science and Engineering C, 2017; 72: 415–424

78. Koc K, Karakus B, Rajar K, Alveroglu E, Synthesis and characterization of ZnS@Fe3O4 fluorescentmagnetic bifunctional nanospheres, Superlattices and Microstructures, 2017; 110: 198-204.

79. Koktysh D, Bright V, Pham W, Fluorescent magnetic hybrid nanoprobe for multimodal bioimaging, Nanotechnology, 2011; 22: 275606.

80. Li K, Ding D, Huo D , Pu KY, Thao NNP, Hu Y, Li Z, Liu B, Conjugated Polymer Based Nanoparticles as Dual-Modal Probes for Targeted In Vivo Fluorescence and Magnetic Resonance Imaging, Adv. Funct. Mater., 2012; 22: 3107–3115.

886 81. Lou L, Yu K, Zhang Z, Li B, Zhu J, Wang Y, Huang R, Zhu Z, Functionalized magnetic-
887 fluorescent hybrid nanoparticles for cell labelling, Nanoscale, 2011; 3: 2315-2323.

888 82. Vargas JM, McBride AA, Plumley JB, Fichou Y, Memon TA, Shah V, Cook NC, Akins BA,
889 Rivera AC, Smolyakov GA, O'Brien JR, Adolphi NL, Smyth HDC, Osin´ sk M, Synthesis and
890 characterization of core/shell Fe3O4/ZnSe fluorescent magnetic nanoparticles, Journal of applied physics,
891 2011; 109: 07B536.

892 83. Wang D, He J, Rosenzweig N, Rosenzweig Z, Superparamagnetic Fe2O3 Beads-CdSe/ZnS
893 Quantum Dots Core-Shell Nanocomposite Particles for Cell Separation, Nano Lett., 2004; 4: 409-413

894 84. Wang K, Ruan J, Qian Q, Song H, Bao C, Zhang X, BRCAA1 monoclonal antibody conjugated
895 fluorescent magnetic nanoparticles for in vivo targeted magnetofluorescent imaging of gastric cancer,
896 Journal of Nanobiotechnology, 2011; 9: 23.

897 85. Wen CY, Xie HY, Zhang ZL, Wu LL, Hu J, Tang M, Fluorescent/magnetic micro/nano-spheres
898 based on quantum dots and/or magnetic nanoparticles: preparation, properties, and their applications in
899 cancer studies, Nanoscale, 2016: 8; 12406-12429.

900 86. Ye F, Barrefelt A, Asem H, Abedi-Valugerdi M, El-Serafi I, Saghafian M, Biodegradable
901 polymeric vesicles containing magnetic nanoparticles, quantum dots and anticancer drugs for drug
902 delivery and imaging, Biomaterials, 2014; 35: 3885-3894.

903 87. Yin N, Wu P, Liang G, Cheng W, A multifunctional mesoporous Fe3O4/SiO2/CdTe magnetic-
904 fluorescent composite nanoprobe, Appl. Phys. A, 2016; 122: 243.

905 88. Gao J, Zhang W, Huang P, Zhang B, Zhang X, Xu B, Intracellular Spatial Control of Fluorescent
906 Magnetic Nanoparticles, J. Am. Chem. Soc., 2008; 130: 3710-3711.

89. Sun L, Zang Y, Sun M, Wang H, Zhu X, Xu S, Yang Q, Li Y, Shan Y, Synthesis of magnetic and fluorescent multifunctional hollow silica nanocomposites for live cell imaging, Journal of Colloid and Interface Science, 2010; 350: 90–98.

90. Gao Y, Zou X , Zhao JX , Li Y , Su X , Graphene oxide-based magnetic fluorescent hybrids for drug delivery and cellular imaging, Colloids and Surfaces B: Biointerfaces, 2013; 112: 128–133.

91. Gaponik N, Radtchenko IL, Sukhorukov GB, Rogach AL, Luminescent Polymer Microcapsules Addressable by a Magnetic Field, Langmuir, 2004; 20: 1449-1452.

92. Efros AL, Nesbitt DJ, Origin and control of blinking in quantum dots, Nature Nanotechnology, 2016; 11: 661-671.

93. Gai S, Yang P, Li C, Wang W, Dai Y, Niu N, Lin J, Synthesis of Magnetic, Up-Conversion Luminescent, and Mesoporous Core–Shell-Structured Nanocomposites as Drug Carriers, Adv. Funct. Mater., 2010; 20: 1166–1172.

94. Mi C, Zhang J, Gao H, Wu X, Wang M, Wu Y, Di Y, Xu Z, Mao C, Xu S, Multifunctional nanocomposites of superparamagnetic (Fe3O4) and NIR-responsive rare earth-doped up-conversion fluorescent (NaYF4 : Yb,Er) nanoparticles and their applications in biolabeling and fluorescent imaging of cancer cells, Nanoscale, 2010; 2: 1141–1148.

95. Borgohain C, Senapati KK, Mishra D, Sarmac KC, Phukan P, A new CoFe2O4–Cr2O3–SiO2 fluorescent magnetic nanocomposite, Nanoscale, 2010; 2: 2250–2256.

96. Wang Y, Cui H, Li K, Sun C, Du W, Cui J, Zhao X, Chen W, A Magnetic Nanoparticle-Based Multiple-Gene Delivery System for Transfection of Porcine Kidney Cells, Plos One, 2014; 9: e102886.

97. Chen D, Jiang M, Li N, Gu H, Xu Q, Ge J, Xia X, Lu J, Modification of magnetic silica/iron oxide nanocomposites with fluorescent polymethacrylic acid for cancer targeting and drug delivery, J. Mater. Chem., 2010; 20: 6422–6429.

98. Huang P, Li Z, Lin J, Yang D, Gao G, Xu C, Photosensitizer-conjugated magnetic nanoparticles for in vivo simultaneous magnetofluorescent imaging and targeting therapy, Biomaterials, 2011; 32: 3447-3458.

99. Pfaff A, Schallon A, Ruhland TM, Majewski AP, Schmalz H, Freitag R, Muller AHE, Magnetic and Fluorescent Glycopolymer Hybrid Nanoparticles for Intranuclear Optical Imaging, Biomacromolecules, 2011; 12: 3805−3811.

100. Janczewski D, Zhang Y, Das GK,2 Yi DK, Padmanabhan P, Bhakoo KK, Tan TTY, Selvan ST, Bimodal Magnetic–Fluorescent Probes for Bioimaging, Microscopy Research and Technique, 2011; 74: 563–576.

101. Wang H, Mu Q, Revia R,, Wang K, Tian B, Lin G, Iron oxide-carbon core-shell nanoparticles for dual-modal imaging-guided photothermal therapy, Journal of Controlled Release, 2018; 289: 70–78.

102. Badruddoza AZ, Rahman T, Ghosh S, Hossain Z, Shi J, Hidajat K, Uddin MS, β-Cyclodextrin conjugated magnetic, fluorescent silica core–shell nanoparticles for biomedical applications, Carbohydrate Polymers, 2013; 95: 449– 457.

103. Yan K, Li H, Li P, Zhu H, Shen J, Yi C, Wu S, Yeung KWK, Xu Z, Xu H, Chu PK, Self-assembled magnetic fluorescent polymeric micelles for magnetic resonance and optical imaging, Biomaterials, 2014; 35: 344-355.

104. McCarthy JE, Prina-Mello A, Rakovich T, Volkov Y, Gun'ko YK, Fabrication and characterization of multimodal magnetic–fluorescent polystyrene nanowires as selective cell imaging probes, J. Mater. Chem., 2011; 21: 14219-14225.

105. Wate PS, Banerjee SS, Jalota-Badhwar A, Mascarenhas RR, Zope KR, Khandare J, Cellular imaging using biocompatible dendrimer-functionalized graphene oxide-based fluorescent probe anchored with magnetic nanoparticles, Nanotechnology, 2012; 23: 415101.

106. Zhou X, Chen L, Wang A, Ma Y, Zhang H, Zhu Y, Multifunctional fluorescent magnetic nanoparticles for lung cancerstem cells research, Colloids and Surfaces B: Biointerfaces, 2015; 134: 431–439.

107. Motlagh NSH, Parvin P, Ghasemi F, Atyabi F, Fluorescence properties of several chemotherapy drugs: doxorubicin, paclitaxel and bleomycin, Biomedical optics express, 2016; 7: 262744

108. Li T, Wu X, Liu F, Li N, Analytical methods based on the light-scattering of plasmonic nanoparticles at the single particle level with dark-field microscopy imaging, Analyst, 2017; 142: 248-256.

109. Yoon GJ, Lee SY, Lee SB, Park GY, Choi JH, Synthesis of Iron Oxide/Gold Composite Nanoparticles Using Polyethyleneimine as a Polymeric Active Stabilizer for Development of a Dual Imaging Probe, Nanomaterials, 2018; 8: 300.

110. De Wilde Y, Lemoine PA, Review of NSOM Microscopy for Materials, AIP Conference Proceedings, 2007; 931: 43-52.

111. Zhang Y, Yazdanpanah V, Yang M, Ozkan M, Ozkan CS, Normal and Cancer Breast Epithelial Cells Endocytosis Study of Nanoparticles by Combined AFM and NSOM Microscopy, Proceedings of the 7th IEEE International Conference on Nanotechnology, 2007; August 2 - 5, Hong Kong.

112. Zhang x, Gaber S, Gaber D, Raman Spectroscopy, Review, International Journal of Engineering and Technical Research (IJETR), 2016; 6: 2321-0869 (O) 2454-4698 (P).

971 113. Pang Y, Wang C, Wang J, Sun Z, Xiao R, Wang S, Fe3O4@Ag magnetic nanoparticles for
972 microRNA capture and duplex-specific nuclease signal amplification based SERS detection in cancer
973 cells, Biosensors and Bioelectronics, 2016; 79: 574–580.

974 114. Xue T, Wang S, Ou G, Li Y, Ruan H, Li Z, Ma Y, Zou R, Qiu J, Shen Z, Wu A, Detection of
975 circulating tumor cells based on improved SERS-active magnetic nanoparticles, Anal.Methods, 2019; 11:
976 2918-2928.

977 115. Zong S, Wang L, Chen C, Lu J, Zhu D, Zhang Y, Wang Z, Cui Y, Facile detection of tumor-
978 derived exosomes using magnetic nanobeads and SERS nanoprobes, Anal. Methods, 2016; 8: 5001-5008.

979 116. Combs CA, Fluorescence Microscopy: A Concise Guide to Current Imaging Methods, Curr Protoc
980 Neurosci, 2010; 79:2.1.1-2.1.25

981 117. Kim MY, Ahn JP, Han SY, Lee NS, Jeong YG, Kim DK, Highly Luminescent and Anti-
982 Photobleaching Core-Shell Structure of Mesoporous Silica and Phosphatidylcholine Modified
983 Superparamagnetic Iron Oxide Nanoparticles, Nanomaterials 2020; 10: 1312.

984 118. Zhang XF, Clime L, Ly HQ, Trudeau M, Veres T, Multifunctional Fe3O4-Au/Porous
985 Silica@Fluorescein Core/Shell Nanoparticles with Enhanced Fluorescence Quantum Yield, J. Phys.
986 Chem. C 2010; 114: 18313–18317.

987 119. Zhang P, Hu C, Ran W, Meng J, Yin Q, Li Y, Recent Progress in Light-Triggered
988 Nanotheranostics for Cancer Treatment, Theranostics, 2016; 6: 948-968.

989 120. Yoo MK, Kim IY, Kim EM, Jeong HJ, Lee, CM, Jeong, YY, Superparamagnetic Iron Oxide
990 Nanoparticles Coated with Galactose-Carrying Polymer for Hepatocyte Targeting, Journal of
991 Biomedicine and Biotechnology, 2007; Article ID 94740.

121. Huang B, Bates M, Zhuang X, Super resolution fluorescence microscopy, Annu Rev Biochem. 2009; 78: 993–1016.

122. Guggenheim EJ, Khan A, Pike J, Chang L, Lynch I, Rappoport JZ, Comparison of Confocal and Super-Resolution Reflectance Imaging of Metal Oxide Nanoparticles, PLoS ONE; 11: e0159980.

123. Heger Z, Cernei N, Krizkova S, Masarik M, Kopel P, Hodek P, Zitka O, Adam V, Kizek R, Paramagnetic Nanoparticles as a Platform for FRET-Based Sarcosine Picomolar Detection, Scientific Reports, 2015, 5 : 8868.

124. Mao Y, Zhang Y, Hu W, Ye W, Carbon Dots-Modified Nanoporous Membrane and Fe3O4@Au Magnet Nanocomposites-Based FRET Assay for Ultrasensitive Histamine Detection, Molecules, 2019; 24, 3039.

125. Cheng Z, Dai Y, Kang X, Li C, Huang S, Lian H, Hou Z, Ma P, Lin J, Gelatin-encapsulated iron oxide nanoparticles for platinum (IV) prodrug delivery, enzyme-stimulated release and MRI, Biomaterials, 2014; 35: 6359-6368.

126. Yang P, Xu QZ, Jin SY, Zhao Y, Lu Y, Xu XW, Yu SH, Synthesis of Fe3O4@Phenol Formaldehyde Resin Core–Shell Nanospheres Loaded with Au Nanoparticles as Magnetic FRET Nanoprobes for Detection of Thiols in Living Cells, Chem. Eur. J., 2012; 18: 1154–1160.

127. Basuki JS, Duong HTT, Macmillan A, Erlich RB, Esser L, Akerfeldt, MC, Using Fluorescence Lifetime Imaging Microscopy to Monitor Theranostic Nanoparticle Uptake and Intracellular Doxorubicin Release, ACS Nano, 2013; 7: 10175–10189.

128. Bothun GD, Preiss MR, Bilayer heating in magnetite nanoparticle–liposome dispersions via fluorescence anisotropy, Journal of Colloid and Interface Science, 2011; 357: 70–74.

129. Lin FC, Zink JI, Probing the Local Nanoscale Heating Mechanism of a Magnetic Core in Mesoporous Silica Drug-Delivery Nanoparticles Using Fluorescence Depolarization, J. Am. Chem. Soc. 2020; 142: 5212−5220.

130. Kwon J, Jun SW, Choi SI, Mao X, Kim J, Koh EK, FeSe quantum dots for in vivo multiphoton biomedical imaging, Sci. Adv., 2019; 5: eaay0044.

131. Seemann KM, Kuhn B, Multi-photon excited luminescence of magnetic FePt core-shell nanoparticles, Biomedical optics express, 2014; 5: 210319.

132. Liao MY, Wu CH, Lai PS, Yu J, Lin HP, Liu TM, Surface State Mediated NIR Two-Photon Fluorescence of Iron Oxides for Nonlinear Optical Microscopy, Adv. Funct. Mater. 2013; 23: 2044–2051.

133. Zhang Y, Zhang B, Liu F, Luo J, Bai J, In vivo tomographic imaging with fluorescence and MRI using tumor-targeted dual-labeled nanoparticles, International Journal of Nanomedicine, 2014; 9: 33–41.

134. Wang G, Zhang X, Liu Y, Hu Z, Mei X, Uvdal K, Magneto-fluorescent nanoparticles with highintensity NIR emission, T1- and T2-weighted MR for multimodal specific tumor imaging, J. Mater. Chem. B, 2015; 3: 3072-3080.

135. Zhang L, Zhang L, Mason RP, Sarkaria JN, Zhao D, Convertible MRI contrast: Sensing the delivery and release of antiglioma nano-drugs, Scientific Reports, 2015; 5: 09874.

136. Ma T, Hou Y, Zeng J, Liu C, Zhang P, Jing L, Shangguan D, Gao M, Dual-Ratiometric Target-Triggered Fluorescent Probe for Simultaneous Quantitative Visualization of Tumor Microenvironment Protease Activity and pH in Vivo, J. Am. Chem. Soc, 2018; 140: 211−218.

137. Domagalski JT, Xifre-Perez E, Tabrizi MA, Ferre-Borrull J, Marsal LF, Magnetic nanoparticle decorated anodic alumina nanotubes for fluorescent detection of cathepsin B, Journal of Colloid and Interface Science, 2021; 584: 236–245.

138. Du J, Zhang Y, Jin Z, Wu H, Cang J, Shen Y, Miao F, Zhang A,, Zhang A, Zhang J, Teng G, Targeted NIRF/MR dual-mode imaging of breast cancer brain metastasis using BRBP1-functionalized ultra-small iron oxide nanoparticles, Materials Science & Engineering C, 2020; 116: 111188.

139. Esfandyari J, Shojaedin-Givi B, Hashemzadeh H, Mozafari-Nia M, Vaezi Z, Naderi-Manesh H, Capture and detection of rare cancer cells in blood by intrinsic fluorescence of a novel functionalized diatom, Photodiagnosis and Photodynamic Therapy, 2020; 30: 101753.

140. Frtús A, Smolková B, Uzhytchak M, Lunova M, Jirsa M, Kubinová S, Dejneka A, Lunov O, Analyzing the mechanisms of iron oxide nanoparticles interactions with cells: A road from failure to success in clinical applications, Journal of Controlled Release, 2020; 328: 59–77.

141. He S, Li J, Lyu Y, Huang J, Pu K, Near-Infrared Fluorescent Macromolecular Reporters for Real-Time Imaging and Urinalysis of Cancer Immunotherapy, J. Am. Chem. Soc. 2020; 142: 7075−7082.

142. Norouzi M, Yathindranath V, Thliveris JA, Kopec BM, Siahaan TJ, Miller DW, Doxorubicin-loaded iron oxide nanoparticles for glioblastoma therapy: a combinational approach for enhanced delivery of nanoparticles, Scientific Reports, 2020; 10: 11292.

143. Reichel D, Sagong B, The J, Zhang Y, Wagner S, Wang H, Chung LWK, Butte P, Black KL, Yu JS, Perez JM, Near Infrared Fluorescent Nanoplatform for Targeted Intraoperative Resection and Chemotherapeutic Treatment of Glioblastoma, ACS Nano 2020; 14: 8392−8408.

144. Shi Y, Wang J, Liu J, Lin G, Xie F, Pang X, Pei Y, Cheng Y, Zhang Y, Lin Z, Yin Z, Wang X, Niu G, Chen X, Liu G, Oxidative stress-driven DR5 upregulation restores TRAIL/Apo2L sensitivity induced by iron oxide nanoparticles in colorectal cancer, Biomaterials 2020; 233: 119753.

145. Tam J, Pilozzi A, Mahmood U, Huang X, Simultaneous Monitoring of Multi-Enzyme Activity and Concentration in Tumor Using a Triply Labeled Fluorescent In Vivo Imaging Probe, Int. J. Mol. Sci. 2020; 21: 3068.

146. Xu Y, Wu H, Huang J, Qian W, Martinson DE, Ji B, Li Y, Wang YA, Yang L, Mao H, Probing and Enhancing Ligand-Mediated Active Targeting of Tumors Using Sub-5 nm Ultrafine Iron Oxide Nanoparticles, Theranostics 2020; 10: 2479-2494.

147. Yildirim T, Pervez M, Li B, O'Reilly RK, Size-controlled clustering of iron oxide nanoparticles within fluorescent nanogels using LCST-driven self-assembly, J. Mater. Chem. B, 2020; 8: 5330-5335.

148. Arsalani S, Oliveira J, Guidelli EJ, Araujo JFDF, Wiekhorst F, Baffaa O, Synthesis of radioluminescent iron oxide nanoparticles functionalized by anthracene for biomedical applications, Colloids and Surfaces A, 2010; 602: 125105.

149. Kima D, Lee YD, Jo S, Kim S, Lee TS, Detection and imaging of cathepsin L in cancer cells using the aggregation of conjugated polymer dots and magnetic nanoparticles, Sensors & Actuators: B. Chemical, 2020; 307: 127641.

150. Pandey N, Menon JU, Takahashi M, Hsieh JT, Yang J, Nguyen KT, Wadajkar AS, Thermo-responsive Fluorescent Nanoparticles for Multimodal Imaging and Treatment of Cancers, Nanotheranostics, 2020; 4: 1-13.

151. Zhi D, Yang T, Yang J, Fu S, Zhang S, Targeting strategies for superparamagnetic iron oxide nanoparticles in cancer therapy, Acta Biomaterialia, 2020; 102: 13–34.

152. Fernández-Lázaro D, Hernández JLG, García AC, Del Castillo AC, Hueso MV, Cruz-Hernández JJ, Clinical Perspective and Translational Oncology of Liquid Biopsy, Diagnostics, 2020; 10: 443.

153. Zhou B, Xu K, Zheng X, Chen T, Wang J, Song Y, Shao Y, Zheng S, Application of exosomes as liquid biopsy in clinical diagnosis, Signal Transduction and Targeted Therapy, 2020; 5: 144.

154. Chang ZM, Wang Z, Shao D, Yue J, Xing H, Li L, Ge M, Li M, Yan H, Hu H, Xu Q, Dong WF, Shape Engineering Boosts Magnetic Mesoporous Silica Nanoparticle-Based Isolation and Detection of Circulating Tumor Cells, ACS Appl. Mater. Interfaces, 2018; 10: 10656−10663.

155. Brancaleon L, Durkin AJ, Tu JH, Menaker G, Fallon JD, Kollias N, In vivo Fluorescence Spectroscopy of Nonmelanoma Skin Cancer, Photochemistry and Photobiology, 2001; 73: 178–183.

156. Ahmed S, Galle PR, Neumann H, Molecular endoscopic imaging: the future is bright, Ther Adv Gastrointest Endosc, 2019; 12: 1–15.

157. Dai X, Qian W, Yang H, Yang L, Jiang H, Targeted Molecular Imaging of Pancreatic Cancer with a Miniature Endoscope, Appl. Sci., 2017; 7: 1241.

158. Yao K, The endoscopic diagnosis of early gastric cancer, Annals of Gastroenterology, 2013; 26: 11-22.

159. Evans JA, Early DS, Chandraskhara V, Chathadi KV, Fanelli RD, Fisher DA, Foley KQ, Hwang JH, Jue TL, Pasha SF, Sharaf R, Shergill AK, Dominitz JA, Cash BD, The role of endoscopy in the assessment and treatment of esophageal cancer, Gastrointestinal endoscopy, 2013; 77: 328-334.

160. Aslim EJ, Lee FJ, Gan VHL, The Utility of Intraoperative Near Infrared Fluorescence (NIR) Imaging with Indocyanine Green (ICG) for the Assessment of Kidney Allograft Perfusion, Journal of Transplantation, 2018; Article ID 6703056.

161. Augurio A, Cortelletti P, Tognato R, Rios A, Levato R, Malda J, Alini M, Eglin D, Giancane G, Speghini,A, Serra T, A Multifunctional Nanocomposite Hydrogel for Endoscopic Tracking and Manipulation, Adv. Intell. Syst., 2020; 2: 1900105.

162. Bae SM, Bae DJ, Do EJ, Oh G, Yoo SW, Lee GJ, Multi-Spectral Fluorescence Imaging of Colon Dysplasia In Vivo Using a Multi-Spectral Endoscopy System, Translation Oncology, 2019; 12: 226-235.

163. Corem-Salkmon E, Perlstein B, Margel S, Design of near-infrared fluorescent bioactive conjugated functional iron oxide nanoparticles for optical detection of colon cancer, International Journal of Nanomedicine, 2012; 7: 5517–5527.

164. Kalyane D, Raval N, Maheshwari R, Tambe V, Kalia K, Tekade RK, Employment of enhanced permeability and retention effect (EPR): Nanoparticle-based precision tools for targeting of therapeutic and diagnostic agent in cancer, Materials Science & Engineering C, 2019; 98: 1252–1276.

165. Liu X, Chen Q, Yang G, Zhang L, Liu Z, Cheng Z, Zhu X, Magnetic nanomaterials with near-infrared pH activatable fluorescence via iron-catalyzed AGET ATRP for tumor acidic microenvironment imaging, J. Mater. Chem. B, 2015; 3: 2786-2800.

166. Park J, Kadasala NR, Abouelmagd SA, Castanares MA, Collins DS, Wei A, Polymer–iron oxide composite nanoparticles for EPR-independent drug delivery, Biomaterials, 2016; 101: 285–295.

167. Han C, Zhang A, Kong Y, Yu N, Xie T, Dou B, Li K, Wang Y, Li J, Xu K, Multifunctional iron oxide-carbon hybrid nanoparticles for targeted fluorescent/MR dual-modal imaging and detection of breast cancer cells, Analytica Chimica Acta, 2019; 1067: 115-128.

168. Landmark KJ, DiMaggio S, Ward J, Kelly C, Vogt S, Hong S, Kotlyar A, Myc A, Thomas TP, Penner-Hahn JE, Baker JR, Holl MMB, Orr BG, Synthesis, Characterization, and in Vitro Testing of Superparamagnetic Iron Oxide Nanoparticles Targeted Using Folic Acid-Conjugated Dendrimers, ACS Nano, 208; 2: 773–783.

169. Peng XH, Qian X, Mao H, Wang AY, Chen Z, Nie S, Shin DM, Targeted magnetic iron oxide nanoparticles for tumor imaging and therapy, International Journal of Nanomedicine, 2008; 3: 311–321.

170. Xia H, Tong R, Song Y, Xiong F, Li J, Wang S, Fu H, Wen J, Li D, Zeng Y, Zhao Z, Wu J, Synthesis and bio applications of targeted magnetic-fluorescent composite nanoparticles, J Nanopart Res, 2017; 19:149.

171. Ikeda H, Ishii A, Sano K, Chihara H, Arai D, Abekura Y, Activatable Fluorescence Imaging of Macrophages in Cerebral Aneurysms Using Iron Oxide Nanoparticles Conjugated With Indocyanine Green, Frontiers in Neuroscience, 2020; 14, Article 370.

172. Zhang L, Wang T, Li L, Wang C, Su Z, Li J, Multifunctional fluorescent-magnetic polyethyleneimine functionalized Fe3O4–mesoporous silica yolk–shell nanocapsules for siRNA delivery. Chem. Commun. 2012; 48: 8706–8708.

173. Vahrmeijer AL, Hutteman M, Van der Vorst JR, Van de Velde CJH, Frangioni JV, Image-guided cancer surgery using near-infrared fluorescence, Nat Rev Clin Oncol., 2013; 10: 507–518.

174. Guo L, Zhang X, Wei R, Li G, Sun B, Zhang H, Liu D, Wang C, Feng M, Engineering microglia as intraoperative optical imaging agent vehicles potentially for fluorescence-guided surgery in gliomas, Biomater. Sci., 2020; 8: 1117-1126.

175. Mangeolle T, Yakavets Y, Marchal S, Debayle M, Pons T, Bezdetnaya L, Marchal F, Fluorescent Nanoparticles for the Guided Surgery of Ovarian Peritoneal Carcinomatosis, Nanomaterials, 2018; 8: 572.

176. Bhattarai P, Hameed S, Dai Z, Recent advances in anti-angiogenic nanomedicines for cancer therapy, Nanoscale, 2018; 10: 5393.

177. Lee S, Thomas RG, Moon MJ, Park HJ, Park IK, Lee BI, Near-Infrared Heptamethine Cyanine Based Iron Oxide Nanoparticles for Tumor Targeted Multimodal Imaging and Photothermal Therapy, Scientific Reports, 2018; 7.

178. Song S, Shen H, Yang T, Wang L, Fu H, Chen H, Indocyanine Green Loaded Magnetic Carbon Nanoparticles for Near Infrared Fluorescence/Magnetic Resonance Dual-Modal Imaging and Photothermal Therapy of Tumor, ACS Appl. Mater. Interfaces 2017; 9: 9484−9495.

179. Li L, Nurunnabi M, Nafiujjaman M,Jeong YY, Lee YK, Huh KM, A photosensitizer-conjugated magnetic iron oxide/gold hybrid nanoparticle as an activatable platform for photodynamic cancer therapy, J. Mater. Chem. B, 2014; 2: 2929-2937.

180. Van Straten D, Mashayekhi V, De Bruijn HS, Oliveira S, Robinson DJ, Oncologic Photodynamic Therapy: Basic Principles, Current Clinical Status and Future Directions, Cancers, 2017; 9: 19.

181. Amirshaghaghi A, Yan L, Miller J, Daniel Y, Stein JM, Busch TM, Cheng Z, Tsourkas A, Chlorin e6-Coated Superparamagnetic Iron Oxide Nanoparticle (SPION) Nanoclusters as a Theranostic Agent for Dual-Mode Imaging and Photodynamic Therapy, Scientific Reports, 2019; 9: 2613.

182. Yin T, Zhang Q, Wu H, Gao G, Shapter JG, Shen Y, He Q, Huang P, Qi W, Cui D, In vivo high-efficiency targeted photodynamic therapy of ultra-small Fe3O4@polymer-NPO/PEG-Glc@Ce6 nanoprobes based on small size effect, NPG Asia Materials, 2017; 9: e383.

183. Mandawala C, Chebbi I, Durand-Dubief M, Le Fèvre R, Hamdous Y, Guyot F, Alphandéry E, Biocompatible and stable magnetosome minerals coated with poly-L-lysine, citric acid, oleic acid, and carboxy-methyl-dextran for application in the magnetic hyperthermia treatment of tumors, J. Mater. Chem. B, 2017; 5: 7644-7660.

184. Hamdous Y, Chebbi I, Mandawala C, Le Fèvre R, Guyot F, Seksek O, Alphandéry E, Biocompatible coated magnetosome minerals with various organization and cellular interaction properties induce cytotoxicity towards RG-2 and GL-261 glioma cells in the presence of an alternating magnetic field, J Nanobiotechnol, 2017; 15: 74.

185. Alphandéry E, A discussion on existing nanomedicine regulation: Progress and pitfalls, Applied Materials Today, 2019; 17: 193–205.

186. Alphandéry E, Applications of magnetotactic bacteria and magnetosome for cancer treatment: A review emphasizing on practical and mechanistic aspects, Drug Discovery Today, 2020; 25: 1444-1452.

187. Kaewsaneha C, Bitar A, Tangboriboonrat P, Polpanich D, Elaissari A, Fluorescent-magnetic Janus particles prepared via seed emulsion polymerization, Journal of Colloid and Interface Science, 424; 98–103 (2014).

188. Lee JY, Chen KJ, Noh SH, Garcia MA, Wang H, Lin WY, Jeong H, Kong BJ, Stout DB, Cheon J, Tseng HR, On-Demand Drug Release System for In Vivo Cancer Treatment through Self-Assembled Magnetic Nanoparticles, Angew. Chem. Int. Ed., 2013; 52: 4384 –4388.

189. Li L, Liu C, Zhang L, Wang T, Yu H, Wang C, Multifunctional magnetic–fluorescent eccentric-(concentric-Fe3O4@SiO2)@polyacrylic acid core–shell nanocomposites for cell imaging and pH-responsive drug delivery, Nanoscale, 2013; 5: 2249-2253.

190. Liu L, Xiao L, Zhu HY, Preparation and characterization of CS Fe3O4@ZnS:Mn magnetic-fluorescent nanoparticles in aqueous media, Chemical Physics Letters, 2012; 539–540: 112–117.

191. Lu Y, Zheng Y, You S, Wang F, Gao Z, Shen J, Li J,Yang W, Yin M, Bifunctional Magnetic-Fluorescent Nanoparticles: Synthesis, Characterization, and Cell Imaging, ACS Appl. Mater. Interfaces, 2015; 7: 5226−5232.

192. Lu Y, He B, Shen J, Li J, Yanga W, Yin M, Multifunctional magnetic and fluorescent core–shell nanoparticles for bioimaging, Nanoscale, 2015; 7: 1606-1609.

193. Mohapatra S, Rout SR, Das RK, Nayak S, Ghosh SK, Highly Hydrophilic Luminescent Magnetic Mesoporous Carbon Nanospheres for Controlled Release of Anticancer Drug and Multimodal Imaging, Langmuir, 2016; 32: 1611−1620.

194. Wang W, Zou M, Chen K, Novel Fe3O4@YPO4 :Re (Re = Tb, Eu) multifunctional magnetic–fluorescent hybrid spheres for biomedical applications, Chem. Commun, 2010; 46: 5100–5102.

195. Wang X, He F, Tang F, Ma N, Li L, Preparation of hybrid fluorescent–magnetic nanoparticles for application to cellular imaging by self-assembly, Colloids and Surfaces A: Physicochem. Eng. Aspects, 2011; 392: 103– 109.

196. Wang F, Chen X, Zhao Z, Tang S, Huang X, Lin C, Synthesis of magnetic, fluorescent and mesoporous core-shell-structured nanoparticles for imaging, targeting and photodynamic therapy, J. Mater. Chem., 2011, 21, 11244-11252.

197. Wang H, Shen J, Li Y, Wei Z, Cao G, Gai Z, Magnetic iron oxide–fluorescent carbon dots integrated nanoparticles for dual-modal imaging, near-infrared light-responsive drug carrier and photothermal therapy, Biomater. Sci., 2014; 2: 915-923.

198. Wang S, Yang W, Du H, Guo F, Wang H, Chang J, Multifunctional reduction-responsive SPIO&DOX-loaded PEGylated polymeric lipid vesicles for magnetic resonance imaging-guided drug delivery, Nanotechnology, 2016; 27: 165101.

199. Xi P, Cheng K, Sun X, Zeng Z, Sun S, Fluorescent magnetic nanoparticles based on a ruthenium complex and Fe3O4, J. Mater. Chem., 2011; 21: 11464–11467.

200. Xi P, Cheng K, Sun X, Zeng Z, Sun S, Magnetic Fe_3O_4 nanoparticles coupled with a fluorescent Eu complex for dual imaging applications, Chem. Commun., 2012; 48: 2952–2954.

201. Xu H, Cheng L, Wang C, Ma X, Li Y, Liu Z, Polymer encapsulated up conversion nanoparticle/iron oxide nanocomposites for multimodal imaging and magnetic targeted drug delivery, Biomaterials, 2011; 32: 9364-9373.

202. Yao Q, Zheng Y, Cheng W, Chen M, Shen J, Yin M, Difunctional fluorescent HSA modified CoFe2O4 magnetic nanoparticles for cell imaging, J. Mater. Chem. B, 2016, 4, 6344-6349.

203. Yen SK, Janczewski D, Lakshmi JL, Dolmanan SB, Tripathy S, Ho VHB, Design and Synthesis of Polymer-Functionalized NIR Fluorescent Dyes Magnetic Nanoparticles for Bioimaging, ACS Nano 2013; 7: 6796–6805.

204. Zhu H, Tao J, Wang W, Zhou Y, Li P, Li Z, Magnetic, fluorescent, and thermo-responsive Fe3O4/rare earth incorporated poly(St-NIPAM) core-shell colloidal nanoparticles in multimodal optical/magnetic resonance imaging probes, Biomaterials, 2013; 34: 2296-2306.